

X-RAY EMISSION PROPERTIES OF LARGE-SCALE JETS, HOT SPOTS, AND LOBES IN ACTIVE GALACTIC NUCLEI

JUN KATAOKA¹ AND ŁUKASZ STAWARZ²

Received 2004 September 6; accepted 2004 December 14

ABSTRACT

We examine a systematic comparison of jet knots, hot spots, and radio lobes recently observed with *Chandra* and *ASCA*. This report discusses the origin of their X-ray emissions and investigates the dynamics of the jets. The data were compiled at well-sampled radio (5 GHz) and X-ray (1 keV) frequencies for more than 40 radio galaxies. We examine three models for the X-ray production: synchrotron (SYN), synchrotron self-Compton (SSC), and external Compton (EC) on cosmic microwave background (CMB) photons. For the SYN sources—mostly jet knots in nearby low-luminosity radio galaxies—X-ray photons are produced by ultrarelativistic electrons with energies 10–100 TeV that must be accelerated in situ. For the other objects, conservatively classified as SSC or EC sources, a simple formulation of calculating the “expected” X-ray fluxes under an equipartition hypothesis is presented. We confirm that the observed X-ray fluxes are close to the expected ones for nonrelativistic emitting plasma velocities in the case of radio lobes and the majority of hot spots, whereas a considerable fraction of jet knots are too bright in X-rays to be explained in this way. We examine two possibilities to account for the discrepancy in a framework of the inverse Compton model: (1) the magnetic field is much smaller than the equipartition value, and (2) the jets are highly relativistic on kiloparsec and megaparsec scales. We conclude that if the inverse Compton model is the case, the X-ray–bright jet knots are most likely far from the minimum-power condition. We also briefly discuss the other possibility, namely, that the observed X-ray emission from all the jet knots is synchrotron in origin.

Subject headings: galaxies: jets — magnetic fields — radiation mechanisms: nonthermal —
radio continuum: galaxies

1. INTRODUCTION

The excellent spatial resolution of the *Chandra X-Ray Observatory* has opened a new era to study the large-scale jets in powerful extragalactic radio sources. At the time of this writing, more than 40 radio-loud active galactic nuclei (AGNs) are known to possess X-ray counterparts of radio jets on kiloparsec to megaparsec scales (Harris & Krawczynski 2002; Stawarz 2005, and references therein).³ Bright X-ray knots (hereafter “jet knots”) are most often detected, but the X-ray emissions from the hot spots and radio lobes are also reported in a number of Fanaroff and Riley type II (FR II) radio galaxies and quasars (e.g., Wilson et al. 2000, 2001; Hardcastle et al. 2002b, 2004; Tashiro et al. 1998; Isobe 2002).

The broadband spectra of jet knots, hot spots, and lobes detected by *Chandra* show great variety between radio and X-ray energy bands. In nearby Fanaroff and Riley type I (FR I) sources, the typical X-ray–to-radio spectrum of the jet knots is consistent with a single, smoothly broken power-law continuum, suggesting that this broadband emission is entirely due to nonthermal synchrotron radiation from a single electron population (e.g., Marshall et al. 2002; Wilson & Yang 2002 for M87). In most other sources, however, the X-ray knots’ spectra are much harder than expected from a simple extrapolation of the radio-to-optical fluxes. In these situations it is believed that both the radio and optical emissions are due to synchrotron radiation, whereas X-ray photons are produced via the inverse Compton scattering of either synchrotron photons (the synchrotron self-Compton [SSC]

process) or cosmic microwave background (CMB) photons (the external Compton [EC] process; Tavecchio et al. 2000; Celotti et al. 2001). Other (synchrotron) models have also been proposed to explain the intense X-ray emission of the large-scale quasar jets (e.g., Dermer & Atoyan 2002; Stawarz & Ostrowski 2002). In the case of the hot spots in powerful sources, one finds an analogous controversy regarding the X-ray emission: although in many objects this emission is consistent with the standard SSC model (see, e.g., Wilson et al. [2000] for Cygnus A), in some other sources it cannot be simply explained in this way, most likely suggesting a synchrotron origin of the detected X-ray photons (see, e.g., Hardcastle et al. 2004). For the extended lobes of quasars and FR II galaxies, it is established that the X-ray radiation is produced by the EC process involving CMB target radiation. In some cases, however, infrared target photons from quasar cores may contribute to the inverse Compton lobes’ emission at keV photon energy ranges (Brunetti et al. 1997).

In the standard picture of FR II radio galaxies and quasars, the relativistic jet is decelerated in a hot spot, converting part of its energy into relativistic electrons and part in a magnetic field. Then the shocked plasma moves inside the head region just behind the hot spot and expands almost adiabatically to form diffuse, extended radio lobes. Although this picture appears to be simple, much of the fundamental physics behind it remains unclear (see, e.g., the recent monograph by De Young 2002b). For example, the velocity and dynamics of the large-scale jets are unknown. From the analogy to subparsec jets in blazar-type AGNs, it is plausible that some of the FR II and quasar jets are highly relativistic even on kiloparsec and megaparsec scales. Recent studies on the optical emission of the large-scale jets seem to justify this hypothesis (e.g., Sparks et al. 1995; Scarpa & Urry 2002; Jester 2003), and the usually discussed versions of the EC model for the X-ray jet knots indeed require the jet

¹ Department of Physics, Tokyo Institute of Technology, 2-12-1, Ohokayama, Meguro, Tokyo 152-8551, Japan; kataoka@hp.phys.titech.ac.jp.

² Obserwatorium Astronomiczne, Uniwersytet Jagielloński, ulica Orła 171, 30-244, Krakow, Poland; stawarz@oa.uj.edu.pl.

³ See also <http://hea-www.harvard.edu/XJET/>.

bulk Lorentz factors $\Gamma_{\text{blk}} \geq 10$ (e.g., Harris & Krawczynski 2002). Yet the exact velocity structure both along and across large-scale jets in FR II radio galaxies and quasars remains an open issue. The strong terminal shocks at the hot spots are unlikely to be moving with high bulk Lorentz factors, but moderately relativistic motions ($\Gamma_{\text{blk}} \leq$ a few) are permitted by hydrodynamic simulations (e.g., Aloy et al. 1999). We note that such simulations repeatedly reveal a complex hot spot morphology, especially at the late stages of the jet evolution (e.g., Martí et al. 1997; Mizuta et al. 2004). Finally, the main-axis expansion of the radio lobe is thought to be subrelativistic; $\Gamma_{\text{blk}} \simeq 1$. However, detailed transport and spatial distribution of the radiating particles within the lobes of powerful radio sources is still being debated (e.g., Blundell & Rawlings 2000; Kaiser 2000; Manolakou & Kirk 2002).

As for the velocity of jet plasma, the strength of the magnetic field in radio galaxies is an open matter. Assuming an equipartition field value in the lobes (1–10 μG), which seems to be supported by observations of the X-ray lobes, a simple flux conservation argument predicts the magnetic field in the jets to be as high as 0.01–1 G (De Young 2002a). Such a strong magnetic field is problematic, since numerical simulations of Poynting-flux-dominated jets (e.g., Komissarov 1999) cannot correctly reproduce the observed large-scale morphologies of powerful radio sources. Thus, an amplification of the magnetic field to the equipartition value in a strong jet terminal shock and in its turbulent downstream region is required, although only a few theoretical investigations of this issue have been reported (see De Young 2002a). Let us mention in this context that turbulent processes that may lead to amplification of the magnetic field can manifest in the formation of the flat-spectrum synchrotron X-ray features, such as the ones discovered recently in the hot spots of the Cygnus A radio galaxy (Bałucińska-Church et al. 2005). On the other hand, the equipartition of energy between the magnetic field and the radiating electrons, established for some high-luminosity sources, may not be valid in general, especially in the case of low-luminosity hot spots (Hardcastle et al. 2004). Finally, we note that the configuration of the magnetic field within the lobes is also not well understood (see a discussion in Blundell & Rawlings 2000).

Unfortunately, present radio-to-X-ray observations are not sufficient to conclusively discriminate between different models proposed in order to explain multiwavelength emission of the large-scale structures of powerful radio sources and of their kiloparsec and megaparsec jets in particular. However, we believe that a systematic comparison between broadband radiative properties of the jet knots, hot spots, and lobes will provide important clues to the dynamics and physics of large-scale jets and put some constraints on the models discussed in the literature. Keeping these motivations in mind, the purpose of this paper is to obtain a rough but unified picture that may link the jet knots, hot spots, and radio lobes rather than to model individual sources in a sufficiently detailed manner. Obviously, detailed studies on individual cases are irreplaceable. In fact, many controversial issues briefly touched in this analysis will remain open until such detailed investigations, based on long multiwavelength observations, are performed. We emphasize that our analysis confirms many results known from the literature (see, e.g., Stawarz 2005 for a review), although for a large number of sources that, in addition, are modeled in a uniform way. Based on this homogeneous approach, however, we explore some new, hardly discussed in the literature, aspects of the physics behind the X-ray emission models for the considered objects. Let us also mention that in this paper we do not consider hadronic models for the

broadband emission of the large-scale jets and their hot spots (see, e.g., Aharonian 2002; Atoyan & Dermer 2004).

Our present study is based on data analysis for a sample consisting of 26 radio galaxies, 14 quasars, and four blazars. We collected all existing data at well-sampled radio (5 GHz) and X-ray (1 keV) frequencies and analyzed them in a systematic manner. In § 2, we define the sample selection and observables used in this paper. In § 3, we present a simple formulation of calculating the “expected” X-ray flux densities for the SSC and EC models taking the relativistic beaming effect into account. We then compare the physical quantities (beaming factor and magnetic field) of the jet knots, hot spots, and lobes. In § 4, we discuss the results, and the summary is presented in § 5.

2. DATA AND ANALYSIS

2.1. Sample

Table 1 compiles a list of X-ray jet sources in which jet knots, hot spots, and/or radio lobes are detected by *Chandra* and *ASCA*. The first pioneer work is reported by Harris & Krawczynski (2002), in which the emission mechanisms of 18 X-ray jet sources (mainly jet knots) are discussed in the framework of a relativistically moving jet model. They continue to maintain current information at the XJET Home Page,⁴ which conveniently summarizes the names, coordinates, distances, and morphologies of the X-ray jet sources. Our sample contains all the sources listed in this page, with additional information on the X-ray observations of radio lobes mainly organized by the *ASCA* team.

Before compiling the data, we performed a quick reanalysis of *Chandra* data (if already archived) to check the published results and found no discrepancy. We therefore refer to published results (fluxes and spectral indexes) unless otherwise stated in this paper. This gives a large number of objects known to us as of 2004 June, which contains 44 X-ray jet sources (56 jet knots, 24 hot spots, and 18 radio lobes; see Table 2). We are aware that our sample is still incomplete, as the known X-ray jet sources are increasing their number day by day. Nevertheless, such a list provides a convenient overview of X-ray jet sources detected so far and a useful hint to *predict* the fluxes of unobserved X-ray jet sources. We also note that Hardcastle et al. (2004) recently summarized the X-ray emission properties of the hot spots in FR II radio galaxies.

The basic information about each source is listed in Table 1: source name (col. [1]), redshift z (col. [2]), luminosity distance to the source d_L adopting $H_0 = 75 \text{ km s}^{-1} \text{ Mpc}^{-1}$ and $q_0 = 0.5$ (col. [3]), classification (col. [4]), and references (col. [5]). RG denotes a radio galaxy of either FR I or FR II, QSO denotes either core-dominated (CD) quasars or lobe-dominated (LD) quasars, and BLZR denotes a blazar-class object.

More detailed information on each source is listed in Table 2. In column (2) we use “knot” (K) to indicate a distinct structure in the jet, “hot spot” (HS) as a terminal bright enhancement at an end of the FR II jet or as one of the multiple features associated with a termination of the jet, and “lobe” (L) as a diffuse extended structure associated with a radio lobe. A suffix after K, HS, and L means the identification of each structure. For example “K-A” denotes “knot A,” and “HS-SE” means “southeast hot spot.” In succeeding columns of Table 2, we list six observables: radio spectral index α_R measured at 5 GHz (col. [3]), radio flux density f_R at 5 GHz in mJy (col. [4]), X-ray spectral index α_X at 1 keV (col. [5]), X-ray flux density f_X at 1 keV in nJy (col. [6]), optical flux density f_o at $5 \times 10^{14} \text{ Hz}$ in μJy (col. [7]),

⁴ Available at <http://hea-www.harvard.edu/XJET/>.

TABLE 1
LIST OF RADIO SOURCES WITH EXTENDED X-RAY JET, HOT SPOT, AND LOBE STRUCTURES

| Name (1) | z (2) | d_L^a (Mpc) (3) | Class ^b (4) | Reference (5) |
|-------------------|------------|-------------------------|---------------------------|------------------|
| 3C 9 | 2.012 | 16133 | QSO (LD) | 1 |
| 3C 15 | 0.073 | 302 | RG (FR I) | 2 |
| NGC 315..... | 0.0165 | 67 | RG (FR I) | 3 |
| 3C 31 | 0.0169 | 67 | RG (FR I) | 4 |
| NGC 612..... | 0.0298 | 120 | RG (FR II) | 5 |
| B0206+35..... | 0.0369 | 150 | RG (FR I) | 6 |
| 3C 66B..... | 0.0215 | 87 | RG (FR I) | 7 |
| Fornax A..... | 0.00587 | 23.5 | RG (FR I) | 8 |
| 3C 120 | 0.033 | 134 | RG (FR II) | 9 |
| 3C 123 | 0.218 | 965 | RG (FR II) | 10 |
| 3C 129 | 0.0208 | 84 | RG (FR I) | 11 |
| Pictor A..... | 0.035 | 143 | RG (FR II) | 5, 12 |
| PKS 0521–365..... | 0.055 | 225 | BLZR | 13 |
| PKS 0637–752..... | 0.653 | 3465 | BLZR | 14 |
| 3C 179 | 0.846 | 4815 | QSO (LD) | 15 |
| B2 0738+313..... | 0.635 | 3344 | QSO (CD) | 16 |
| B2 0755+37..... | 0.0428 | 175 | RG (FR I) | 6 |
| 3C 207 | 0.684 | 3642 | QSO (LD) | 17 |
| 3C 212 | 1.049 | 6393 | QSO (LD) | 18 |
| 3C 219 | 0.174 | 756 | RG (FR II) | 19 |
| 4C 73.08..... | 0.0581 | 236 | RG (FR II) | 5 |
| Q0957+561..... | 1.41 | 9613 | QSO (CD) | 20 |
| 3C 254 | 0.734 | 4011 | QSO (LD) | 21 |
| PKS 1127–145..... | 1.187 | 7505 | QSO (CD) | 22 |
| PKS 1136–135..... | 0.554 | 2830 | QSO (LD) | 15 |
| 3C 263 | 0.656 | 3487 | QSO (LD) | 23 |
| 4C 49.22..... | 0.334 | 1559 | QSO (CD) | 15 |
| M84..... | 0.00354 | 11.3 | RG (FR I) | 24 |
| 3C 273 | 0.1583 | 683 | BLZR | 25 |
| M87..... | 0.00427 | 10.7 | RG (FR I) | 26 |
| 3C 280 | 0.996 | 5964 | RG (FR II) | 21 |
| Cen A..... | 0.00183 | 2.3 | RG (FR I) | 27 |
| Cen B..... | 0.01215 | 48.7 | RG (FR I) | 28 |
| 4C 19.44..... | 0.720 | 3917 | QSO (CD) | 15 |
| 3C 295 | 0.45 | 2205 | RG (FR II) | 29 |
| 3C 303 | 0.141 | 603 | RG (FR II) | 30 |
| GB 1508+5714..... | 4.3 | 54142 | QSO (CD) | 31 |
| 3C 330 | 0.55 | 2803 | RG (FR II) | 23 |
| NGC 6251..... | 0.0249 | 101 | RG (FR I) | 32 |
| 3C 351 | 0.372 | 1763 | QSO (LD) | 23, 33 |
| 3C 371 | 0.051 | 209 | BLZR | 34 |
| 3C 390.3..... | 0.0561 | 230 | RG (FR II) | 35, this work |
| Cygnus A..... | 0.0562 | 231 | RG (FR II) | 36 |
| 3C 452 | 0.0811 | 331 | RG (FR II) | 37 |

^a Luminosity distance to the source adopting $H_0 = 75 \text{ km s}^{-1} \text{ Mpc}^{-1}$ and $q_0 = 0.5$.

^b RG: radio galaxy of either Fanaroff & Riley type I (FR I) or type II (FR II); QSO: quasar, either core-dominated (CD) or lobe-dominated (LD); BLZR: blazar.

REFERENCES.—(1) Bridle et al. 1994; Fabian et al. 2003; (2) Leahy et al. 1997; Kataoka et al. 2003b; (3) Worrall et al. 2003; (4) Laing & Bridle 2002; Hardcastle et al. 2002a; (5) Isobe 2002; (6) Worrall et al. 2001; (7) Hardcastle et al. 2001b; (8) Tashiro et al. 2001; (9) Harris et al. 1999, 2004; (10) Hardcastle et al. 1997, 2001a; (11) Harris et al. 2002b; (12) Wilson et al. 2001; (13) Birkinshaw et al. 2002; (14) Chartas et al. 2000; Schwartz et al. 2000; (15) Sambruna et al. 2002; (16) Siemiginowska et al. 2003b; (17) Brunetti et al. 2002; (18) Akujor et al. 1991; Aldcroft et al. 2003; (19) Comastri et al. 2003; (20) Harvanek et al. 1997; Chartas et al. 2002; (21) Donahue et al. 2003; (22) Siemiginowska et al. 2002; (23) Hardcastle et al. 2002b; (24) Harris et al. 2002a; (25) Marshall et al. 2001; Sambruna et al. 2001; (26) Marshall et al. 2002; Wilson & Yang 2002; Perlman et al. 2001; (27) Kraft et al. 2002; (28) Tashiro et al. 1998; (29) Harris et al. 2000; Brunetti et al. 2001b; (30) Meisenheimer et al. 1997; Kataoka et al. 2003a; (31) Siemiginowska et al. 2003a; Yuan et al. 2003; Cheung 2004; (32) Sambruna et al. 2004; (33) Brunetti et al. 2001a; (34) Pesce et al. 2001; (35) Harris et al. 1998; (36) Wilson et al. 2000; (37) Isobe et al. 2002.

TABLE 2
PARAMETERS FOR X-RAY JET, HOT SPOT, AND LOBE FEATURES

| NAME (1) | COMPONENT (2) | OBSERVABLES ^a | | | | | | MODEL RESULTS ^b | | | | | CLASS ^c (14) |
|----------------|------------------|--------------------------|-----------------------|-------------------|-----------------------|-----------------------------|-----------------------------|----------------------------------|----------------------|---------------------|------------------------|-----------------------|----------------------------|
| | | α_R (3) | f_R (mJy) (4) | α_X (5) | f_X (nJy) (6) | f_o (μ Jy) (7) | θ (arcsec) (8) | $B_{eq}(1)$ (μ G) (9) | $R_{SSC}(1)$ (10) | $R_{EC}(1)$ (11) | δ_{SSC} (12) | δ_{EC} (13) | |
| 3C 9 | K | 1.0 ^d | 3.2E2 | 0.6 ± 0.6 | 2.2 | ... | 0.3 ^d | 230 | 3.6 | 54 | 0.60 | 3.8 | SSC |
| 3C 15 | K-C | 0.9 | 55 | 0.7 ± 0.4 | 1.2 | 6.0 | 0.3 ^d | 84 | 5.5E2 | 1.5E3 | 0.080 | 11 | SYN |
| | L | 0.8 | 1.8E3 | 0.3 ± 0.4 | 2.9 | ... | 20 | 6.2 | 58 | 1.1 | 0.20 | 1.0 | EC |
| NGC 315 | K | 0.9 ^d | 68 | 1.5 ± 0.7 | 4.1 | ... | 0.3 ^d | 130 | 3.1E3 | 1.0E4 | 0.040 | 22 | SYN |
| 3C 31 | K | 0.55 | 37 | 1.1 ± 0.2 | 7.3 | 2.0 | 0.3 ^d | 110 | 1.4E4 | 2.4E4 | 0.022 | 29 | SYN |
| NGC 612 | L | 0.6 | 5.1E3 | 1.0 ± 0.5 | 37 | ... | 120 | 2.2 | 6.4E2 | 0.99 | 0.075 | 0.99 | EC |
| B0206 | K | 0.5 | 26 | 1.1 ± 0.7 | 5.2 | ... | 0.3 ^d | 79 | 1.1E4 | 1.4E4 | 0.024 | 24 | SYN |
| 3C 66B | K-A | 0.75 | 3.9 | 1.0 ± 0.3 | 4.0 | 1.0 | 0.3 ^d | 52 | 1.9E5 | 3.6E4 | 7.7E-3 | 33 | SYN |
| | K-B | 0.60 | 34 | 1.2 ± 0.1 | 6.2 | 15.8 | 0.3 ^d | 97 | 1.2E4 | 1.9E4 | 0.024 | 27 | SYN |
| Fornax A | L | 0.9 | 1.6E4 | 0.7 ± 0.3 | 100 | ... | 450 | 1.5 | 1.4E3 | 0.47 | 0.055 | 0.78 | EC |
| 3C 120 | K | 0.65 | 9.2 | 0.5 ± 0.1 | 29 | <0.7 | 1.5 | 15 | 6.9E5 | 1.2E4 | 4.6E-3 | 23 | EC |
| 3C 123 | HS | 0.5 | 5.2E3 | 0.6 ± 0.3 | 4.6 | <3 | 0.5 | 170 | 1.5 | 1.3E2 | 0.85 | 5.1 | SSC |
| 3C 129 | K | 0.5 ^d | 3.8 | 1.0 ^d | 1.9 | ... | 0.3 ^d | 52 | 9.7E4 | 1.8E4 | 0.010 | 26 | SYN |
| Pic A | HS | 0.74 | 2.0E3 | 1.1 ± 0.1 | 87 | 104 | 0.5 | 180 | 3.6E2 | 1.2E4 | 0.095 | 23 | SYN |
| | L-W | 0.72 | 1.3E4 | 0.6 ± 0.3 | 56 | ... | 90 | 3.5 | 1.9E2 | 1.3 | 0.12 | 1.1 | EC |
| PKS 0521 | K | 0.6 | 1.5E2 | 1.3 ± 0.3 | 14 | 45 | 0.3 ^d | 120 | 1.7E3 | 1.2E4 | 0.050 | 23 | SYN |
| PKS 0637 | K | 0.8 | 48 | 0.9 ± 0.1 | 6.2 | 0.2 | 0.3 ^d | 80 | 6.0E2 | 1.6E3 | 0.077 | 12 | EC |
| 3C 179 | K-A | 0.8 | 73 | 1.0 ^d | 0.40 | <0.06 | 0.3 ^d | 97 | 15 | 61 | 0.34 | 4.0 | EC |
| | K-B | 0.8 | 1.1E2 | 1.0 ^d | 1.1 | <0.06 | 0.3 ^d | 110 | 23 | 1.4E2 | 0.29 | 5.2 | EC |
| | CL | 0.8 ^d | 2.9E2 | 1.0 ^d | 0.24 | <2.8 | 2.0 | 28 | 3.0 | 1.1 | 0.64 | 1.0 | EC |
| B2 0738 | K-A | 0.5 ^d | 1.7 | 0.5 ± 0.4 | 0.30 | ... | 0.3 ^d | 30 | 4.5E3 | 4.1E2 | 0.035 | 7.4 | EC |
| | HS-B1 | 0.5 ^d | 2.2 | 1.0 ± 0.3 | 0.33 | ... | 0.3 ^d | 33 | 3.4E3 | 4.0E2 | 0.039 | 7.4 | SYN |
| | HS-B2 | 0.5 ^d | 4.0 | 1.4 ± 0.5 | 0.10 | ... | 0.3 ^d | 39 | 4.2E2 | 89 | 0.090 | 4.5 | SYN |
| B2 0755 | K | 0.5 ^d | 54 | 1.1 ± 0.2 | 9.7 | ... | 0.3 ^d | 94 | 6.3E3 | 1.6E4 | 0.030 | 25 | SYN |
| 3C 207 | K | 0.8 | 2.3E2 | 0.2 ± 0.3 | 4.6 | ... | 0.3 ^d | 130 | 46 | 5.1E2 | 0.22 | 8.0 | SSC |
| | HS | 0.8 | 1.6E2 | 0.7 ± 1.0 | 1.3 | ... | 0.3 ^d | 110 | 23 | 1.7E2 | 0.29 | 5.6 | SSC |
| | L | 0.9 | 2.5E2 | 0.5 ± 0.4 | 4.5 | ... | 5.0 | 12 | 1.4E2 | 7.0 | 0.14 | 1.9 | EC |
| 3C 212 | HS-S? | 0.5 ^d | 13 | 1.0 ^d | 0.80 | ... | 0.3 ^d | 64 | 3.1E2 | 2.3E2 | 0.10 | 6.1 | SYN |
| | HS-N? | 0.5 ^d | 74 | 1.0 ^d | 0.48 | ... | 0.3 ^d | 106 | 14 | 58 | 0.35 | 3.9 | SYN |
| 3C 219 | L | 0.8 | 2.2E3 | 0.7 ± 0.2 | 30 | ... | 50 | 2.7 | 4.0E2 | 1.6 | 0.091 | 1.2 | EC |
| 4C 73.08 | L-E | 0.85 | 2.7E2 | 0.7 ± 0.4 | 54 | ... | 180 | 0.58 | 6.4E4 | 2.3 | 0.012 | 1.3 | EC |
| | L-W | 0.85 | 5.6E2 | 0.65 ^d | 31 | ... | 180 | 0.71 | 1.2E4 | 0.93 | 0.023 | 0.98 | EC |
| Q0957 | K-B | 0.8 ^d | 2.2E2 | 0.9 ± 0.6 | 0.37 | <0.11 | 0.3 ^d | 170 | 1.7 | 18 | 0.81 | 2.6 | SSC |
| | K-C | 0.8 ^d | 1.3E2 | 0.9 ± 0.6 | 0.11 | <0.11 | 0.3 ^d | 140 | 1.1 | 6.9 | 0.96 | 1.9 | SSC |
| 3C 254 | HS-W | 0.8 ^d | 98 | 1.0 ± 0.8 | 0.52 | ... | 0.3 ^d | 100 | 15 | 81 | 0.34 | 4.3 | SYN |
| PKS 1127 | K-A | 1.2 | 1.3 | 0.5 ^d | 1.1 | ... | 0.3 ^d | 35 | 1.1E4 | 8.6E2 | 0.024 | 9.5 | EC |
| | K-B | 0.82 | 16 | 0.5 ^d | 0.89 | <0.18 | 0.3 ^d | 72 | 2.2E2 | 2.0E2 | 0.11 | 5.8 | EC |
| | K-C | 0.86 | 17 | 0.5 ^d | 0.60 | <0.15 | 0.3 ^d | 73 | 1.3E2 | 1.3E2 | 0.14 | 5.1 | EC |
| PKS 1136 | K-A | 0.8 ^d | 1.0 | 1.0 ^d | 1.41 | 0.23 | 0.3 ^d | 25 | 5.4E4 | 2.9E3 | 0.013 | 14 | EC |
| | K-B | 0.8 ^d | 41 | 1.0 ^d | 3.7 | 0.24 | 0.3 ^d | 73 | 5.4E2 | 1.2E3 | 0.081 | 11 | EC |
| | K-C | 0.8 ^d | 1.9E2 | 1.0 ^d | <0.62 | 0.13 | 0.3 ^d | 110 | <9.1 | <92 | >0.41 | <4.5 | EC |
| 3C 263 | HS-K | 0.8 ^d | 5.7E2 | 1.0 ± 0.1 | 1.0 | 0.8 | 0.3 ^d | 160 | 2.7 | 72 | 0.67 | 4.2 | SSC |
| | HS-B | 0.8 ^d | 22 | 1.0 ^d | <0.06 | ... | 0.3 ^d | 64 | <19 | <22 | >0.31 | <2.8 | SSC |
| | L-NW | 0.8 ^d | 1.9E2 | 0.4 ± 0.2 | 0.8 | ... | 8 | 7.1 | 51 | 0.73 | 0.21 | 0.90 | EC |
| | L-SW | 0.8 ^d | 44 | 0.4 ± 0.2 | 0.5 | ... | 8 | 4.7 | 2.8E2 | 0.95 | 0.10 | 0.98 | EC |
| 4C 49.22 | K-A | 0.8 ^d | 56 | 1.0 ^d | 3.9 | 0.63 | 0.3 ^d | 75 | 5.9E2 | 1.7E3 | 0.08 | 12 | EC |
| | K-B | 0.8 ^d | 36 | 1.0 ^d | 1.3 | 0.02 | 0.3 ^d | 66 | 3.8E2 | 7.0E2 | 0.09 | 8.9 | EC |
| | K-C | 0.8 ^d | 74 | 1.0 ^d | 0.99 | 0.08 | 0.3 ^d | 81 | 98 | 3.7E2 | 0.16 | 7.2 | EC |
| M84 | K-2.5 | 0.65 | 3.5 | 0.8 ± 0.3 | 0.63 | <30 | 0.3 ^d | 88 | 1.0E5 | 1.7E4 | 9.9E-3 | 26 | SYN |
| | K-3.3 | 0.65 | 13 | 0.8 ± 0.3 | 1.16 | <30 | 0.3 ^d | 130 | 2.6E4 | 1.6E4 | 0.02 | 25 | SYN |
| 3C 273 | K-A1 | 0.65 | 20 | 0.6 ± 0.1 | 38.1 | 5.2 | 0.3 ^d | 56 | 4.8E4 | 4.8E4 | 0.01 | 36 | SYN |
| | K-B1 | 0.65 | 2.2E2 | 0.9 ± 0.1 | 23.2 | 5.2 | 0.3 ^d | 110 | 8.1E2 | 8.7E3 | 0.069 | 21 | EC |
| | K-D/H3 | 0.65 | 3.2E2 | 0.8 ± 0.1 | 8.27 | 8.2 | 0.3 ^d | 120 | 1.6E2 | 2.6E3 | 0.13 | 14 | EC |
| M87 | K-HST1 | 0.7 | 77 | 1.3 ± 0.1 | 81.9 | 20 | 0.3 ^d | 220 | 1.3E5 | 4.8E5 | 9.0E-3 | 78 | SYN |
| | K-A | 0.7 | 3.5E2 | 1.3 ± 0.2 | 67.8 | 100 | 0.3 ^d | 330 | 1.1E4 | 1.9E5 | 0.024 | 57 | SYN |
| | K-D | 0.7 | 2.6E3 | 1.6 ± 0.1 | 142 | 1000 | 0.3 ^d | 590 | 1.2E3 | 1.4E5 | 0.059 | 52 | SYN |
| 3C 280 | HS-W | 0.8 | 7.2E2 | 1.3 ± 1.0 | 0.79 | 0.99 | 0.3 ^d | 200 | 0.95 | 32 | 1.0 | 3.2 | SSC |
| | HS-E | 0.8 | 3.3E2 | 1.2 | 0.34 | 0.23 | 0.3 ^d | 160 | 1.3 | 21 | 0.90 | 2.7 | SSC |

TABLE 2—Continued

| NAME (1) | COMPONENT (2) | OBSERVABLES ^a | | | | | | MODEL RESULTS ^b | | | | | |
|---------------|------------------|--------------------------|-----------------------|-------------------|-----------------------|-----------------------------|-----------------------------|----------------------------------|----------------------|---------------------|------------------------|-----------------------|----------------------------|
| | | α_R (3) | f_R (mJy) (4) | α_X (5) | f_X (nJy) (6) | f_o (μ Jy) (7) | θ (arcsec) (8) | $B_{eq}(1)$ (μ G) (9) | $R_{SSC}(1)$ (10) | $R_{EC}(1)$ (11) | δ_{SSC} (12) | δ_{EC} (13) | CLASS ^c (14) |
| Cen A..... | K-NX1 | 0.8 ^d | 36 | 1.5 | 5.8 | ... | 0.3 ^d | 270 | 6.3E4 | 1.1E5 | 0.01 | 48 | SYN |
| | K-AX1 | 0.8 ^d | 5.2E2 | 1.5 | 110 | ... | 0.3 ^d | 580 | 2.2E4 | 5.4E5 | 0.02 | 81 | SYN |
| | K-AX2 | 0.8 ^d | 4.8E2 | 1.5 | 14 | ... | 0.3 ^d | 570 | 3.1E3 | 7.1E4 | 0.04 | 41 | SYN |
| | K-AX3 | 0.8 ^d | 7.4E2 | 1.2 | 28 | ... | 0.3 ^d | 640 | 3.3E3 | 1.1E5 | 0.04 | 49 | SYN |
| | K-AX4 | 0.8 ^d | 3.3E2 | 1.2 | 14 | ... | 0.3 ^d | 510 | 5.5E3 | 8.6E4 | 0.03 | 44 | SYN |
| | K-AX6 | 0.8 ^d | 71 | 1.2 | 23 | ... | 0.3 ^d | 330 | 9.0E4 | 3.0E5 | 0.01 | 67 | SYN |
| | K-BX2 | 0.8 ^d | 88 | 1.0 | 66 | ... | 0.3 ^d | 350 | 1.9E5 | 7.8E5 | 7.8E-3 | 92 | SYN |
| Cen B..... | K-BX5 | 0.8 ^d | 7.5E2 | 1.0 | 50 | ... | 0.3 ^d | 640 | 5.7E3 | 2.0E5 | 0.03 | 59 | SYN |
| | L | 0.78 | 3.7E4 | 0.9 \pm 0.2 | 220 | ... | 180 | 3.5 | 3.8E2 | 1.9 | 0.09 | 1.2 | EC |
| 4C 19.44..... | K-A | 0.8 ^d | 57 | 1.0 ^d | 8.3 | 0.3 | 0.3 ^d | 86 | 5.6E2 | 1.7E3 | 0.08 | 12 | EC |
| | K-B | 0.8 ^d | 23 | 1.0 ^d | 0.24 | 0.04 | 0.3 ^d | 66 | 63 | 79 | 0.19 | 4.3 | EC |
| | K-C | 0.8 ^d | 13 | 1.0 ^d | 0.37 | <0.06 | 0.3 ^d | 56 | 2.3E2 | 1.6E2 | 0.11 | 5.4 | EC |
| | K-D | 0.8 ^d | 16 | 1.0 ^d | 0.25 | <0.06 | 0.3 ^d | 60 | 1.1E2 | 98 | 0.15 | 4.6 | EC |
| | K-E | 0.8 ^d | 6 | 1.0 ^d | 0.25 | <0.06 | 0.3 ^d | 45 | 4.9E2 | 1.6E2 | 0.08 | 5.4 | EC |
| | K-F | 0.8 ^d | 12 | 1.0 ^d | 0.70 | <0.06 | 0.3 ^d | 55 | 4.9E2 | 3.2E2 | 0.08 | 6.8 | EC |
| | K-G | 0.8 ^d | 13 | 1.0 ^d | 0.62 | <0.06 | 0.3 ^d | 56 | 3.8E2 | 2.7E2 | 0.09 | 6.5 | EC |
| | K-H | 0.8 ^d | >1 | 1.0 ^d | 0.41 | <0.06 | 0.3 ^d | >27 | >1.2E4 | >6.4E2 | >0.02 | <8.6 | EC |
| | K-I | 0.8 ^d | 87 | 1.0 ^d | 0.66 | ... | 0.3 ^d | 97 | 24 | 1.1E2 | 0.28 | 4.8 | EC |
| 3C 295..... | HS-NW | 0.65 | 1.3E3 | 0.9 \pm 0.5 | 3.9 | 0.078 | 0.3 ^d | 190 | 4.4 | 2.7E2 | 0.55 | 6.5 | SSC |
| | HS-SE | 0.65 | 6.3E2 | 0.9 \pm 0.5 | 1.1 | <0.02 | 0.3 ^d | 150 | 3.6 | 1.1E2 | 0.60 | 4.8 | SSC |
| | L | 0.9 | 6.5E3 | 0.4 \pm 0.2 | 3.4 | ... | 1.5 | 75 | 0.76 | 9.4 | 1.1 | 2.1 | SSC |
| 3C 303..... | HS | 0.84 | 2.6E2 | 0.4 \pm 0.2 | 4.0 | 7.5 | 1.0 | 42 | 2.2E2 | 2.5E2 | 0.12 | 6.3 | SSC |
| GB 1508..... | K | >0.8 | 0.43 | 0.9 \pm 0.4 | 1.1 | <0.2 | 0.6 | 32 | 1.6E4 | 81 | 0.02 | 4.3 | EC |
| 3C 330..... | HS-NE | 1.0 | 1.3E3 | 0.5 ^d | 0.34 | <0.5 | 0.3 ^d | 200 | 0.32 | 19 | 1.6 | 2.7 | SSC |
| | HS-SW | 1.0 | 1.3E2 | 0.5 ^d | 0.09 | <0.5 | 0.3 ^d | 100 | 2.6 | 16 | 0.68 | 2.5 | SSC |
| | L-NE | 0.9 | 2.6E2 | 0.5 ^d | 0.28 | ... | 3.5 | 15 | 8.9 | 0.90 | 0.42 | 1.0 | EC |
| | L-SW | 1.0 | 2.3E2 | 0.5 ^d | 0.32 | ... | 3.5 | 15 | 12 | 1.1 | 0.37 | 1.0 | EC |
| NGC 6251..... | K | 0.64 | 2.2E2 | 0.2 \pm 0.4 | 2.3 | ... | 10 | 7.9 | 1.4E3 | 13 | 0.06 | 2.4 | EC |
| 3C 351..... | HS-J | 0.7 | 1.9E2 | 0.5 \pm 0.1 | 4.3 | 2.5 | 0.3 ^d | 110 | 1.0E2 | 9.2E2 | 0.16 | 9.7 | SSC |
| | HS-L | 0.7 | 4.5E2 | 0.9 \pm 0.1 | 3.4 | 3.8 | 0.8 | 59 | 36 | 1.1E2 | 0.24 | 4.8 | SSC |
| | HS-A | 0.8 | 4.5 | 0.9 ^d | <0.05 | ... | 0.3 ^d | 37 | <3.0E2 | <69 | >0.10 | <4.1 | SSC |
| | L-N | 1.0 | 72 | 0.6 \pm 0.8 | 1.1 | ... | 10 | 4.0 | 5.9E2 | 2.0 | 0.08 | 1.3 | EC |
| | L-S | 0.9 | 73 | 0.6 \pm 0.8 | 0.7 | ... | 10 | 4.0 | 3.7E2 | 1.3 | 0.09 | 1.1 | EC |
| 3C 371..... | K-A | 0.76 | 37 | 1.0 ^d | 6.7 | 5.8 | 0.3 ^d | 81 | 6.9E3 | 1.2E4 | 0.03 | 23 | SYN |
| | K-B | 0.73 | 15 | 0.7 \pm 0.3 | 16 | 3.4 | 0.3 ^d | 62 | 6.4E4 | 4.6E4 | 0.01 | 36 | SYN |
| 3C 390.3..... | HS-NE-B | 0.7 | 3.5E2 | 0.9 \pm 0.1 | 4.5 | 1.8 | 1.1 | 49 | 2.9E2 | 3.6E2 | 0.10 | 7.1 | SYN |
| | HS-SW | 0.7 | 67 | 0.4 \pm 0.2 | 3.5 | ... | 10 | 4.7 | 8.1E3 | 23 | 0.03 | 2.9 | EC |
| Cygnus A..... | HS-A | 0.55 | 4.0E4 | 0.8 \pm 0.2 | 19 | ... | 1.2 | 180 | 1.0 | 1.3E2 | 0.98 | 5.0 | SSC |
| | HS-D | 0.50 | 5.0E4 | 0.8 \pm 0.2 | 29 | <8 | 1.2 | 190 | 1.2 | 1.7E2 | 0.94 | 5.5 | SSC |
| 3C 452..... | L | 0.78 | 4.0E3 | 0.7 \pm 0.3 | 41 | ... | 80 | 2.4 | 4.7E2 | 1.3 | 0.09 | 1.1 | EC |

^a α_R : radio spectral index at 5 GHz; f_R : radio flux density at 5 GHz; α_X : X-ray spectral index at 1 keV; f_X : X-ray flux density at 1 keV; f_o : optical flux density at 5×10^{14} Hz; θ : radial size of the emitting region.

^b $B_{eq}(1)$: equipartition magnetic field for no beaming ($\delta = 1$); $R_{SSC}(1)$: ratio of observed X-ray flux density to that expected from SSC model for $\delta = 1$; $R_{EC}(1)$: ratio of observed X-ray flux density to that expected from EC model for $\delta = 1$; δ_{SSC} : Doppler beaming factor required to hold equipartition, i.e., $R_{SSC}(\delta_{SSC}) \simeq 1$;

^c Most likely scenario of producing observed X-rays.

^d Assumed to be a listed value.

and radial size θ of the emitting region in arcseconds (col. [8]). When observations have not been reported at 5 GHz or 1 keV, we calculate the flux by extrapolating the nearest measured frequency by assuming the spectral index listed in the table. Values for which we have assumed the fixed value for this calculation are noted.

2.2. Radio/X-Ray Comparison

Figure 1 shows the distribution of the spectral indexes in the radio band (α_R ; *top*) and in the X-ray band (α_X ; *bottom*). Note that the radio spectral index shows a relatively narrow distribution centered at 0.8, and there is no clear difference between the jet knots, hot spots, and radio lobes. As is widely believed,

the radio emissions of these sources are most likely due to the synchrotron radiation from the low-energy population of relativistic electrons. In other words, the energy index of accelerated electrons is narrowly distributed around $s = (\alpha_R + 1)/2 \simeq 2.6$, which is slightly steeper than the one expected from a diffusive acceleration at nonrelativistic shocks, $s = 2$. Let us note in this context that analytical and numerical studies of particle acceleration at relativistic shocks (reviewed by, e.g., Kirk & Duffy 1999; Ostrowski 2002) indicate that in such a case one can expect a variety of particle spectra, with the asymptotic power-law inclination $s = 2.2$ for the strong turbulence condition and ultrarelativistic shock velocity. We also note that stochastic second-order Fermi processes do not favor any universal value

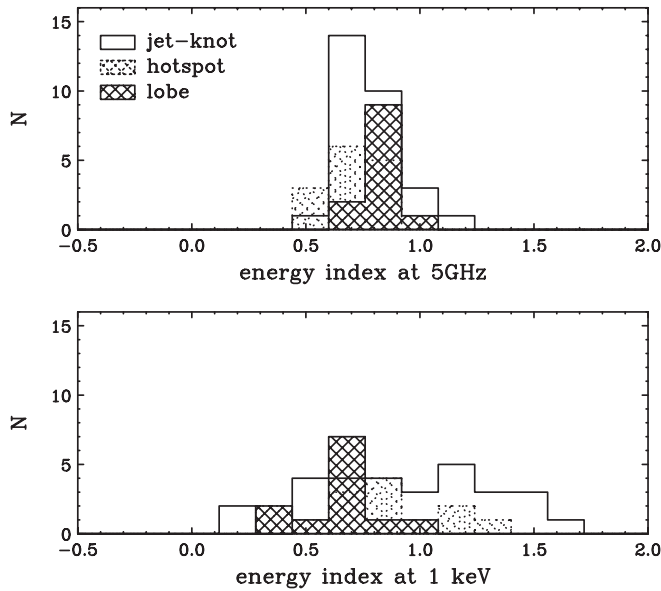


FIG. 1.—Distribution of the energy index measured at 5 GHz (*top*) and 1 keV (*bottom*).

of the power-law spectral index characterizing accelerated electrons.

Meanwhile, the X-ray energy index, α_X , is widely distributed from 0.2 to 1.6. Part of the reason may be relatively large uncertainties in determining the spectral shape of faint X-ray sources compared to the radio spectral shape, but even if only bright (i.e., with small error bars) X-ray sources are plotted, the same trend is obtained. Steep X-ray sources are most frequently found in nearby FR I radio galaxies. As discussed in the literature, the X-ray fluxes in these sources may smoothly connect with radio and/or optical fluxes and hence are considered to be the highest energy tail of the synchrotron radiation. For the X-ray emission from other jet knots, the situation is less clear. Flat X-ray spectral indexes may indicate pileup effects at the high-energy part of the electron energy distribution, thus advocating synchrotron origin of the keV photons (see Harris et al. 2004), or, oppositely, spectral flattenings occurring at the low-energy part of the electron continuum, thus being consistent with the EC interpretation of the X-ray knots' emission. Clearly, spectral information alone is not sufficient at the moment to distinguish between a synchrotron and an inverse Compton origin of the keV photons from the jet knots in most of the cases or to indicate the appropriate particle acceleration process.

Figure 2 presents the distribution of luminosity ratio of L_R and L_X , where $L_R = 4\pi d_L^2 f_R \nu_R$ and $L_X = 4\pi d_L^2 f_X \nu_X$. Note that a clear difference can be seen between the jet knot and hot spot or radio lobes. The jet knots tend to be much brighter in X-rays than the hot spots and radio lobes. This trend is seen more clearly in Figure 3, where the correlation between L_R and L_X is plotted in two-dimensional space. One finds several important tendencies that cannot be accounted for by the sampling bias effect. First, hot spots and radio lobes only occupy the high-luminosity part of the plot, namely $\geq 10^{40}$ ergs s^{-1} . Second, low-luminosity hot spots tend to be brighter in X-rays, as has been pointed out by Hardcastle et al. (2004). Third, $L_R \geq L_X$ for most of the hot spots and radio lobes, but most of the jet knots show an opposite trend.

We should note that because of the limited sensitivity of *Chandra* (typically 0.1 nJy at 1 keV for a 10 ks exposure), we would not expect to detect the X-ray emission from the “X-ray–

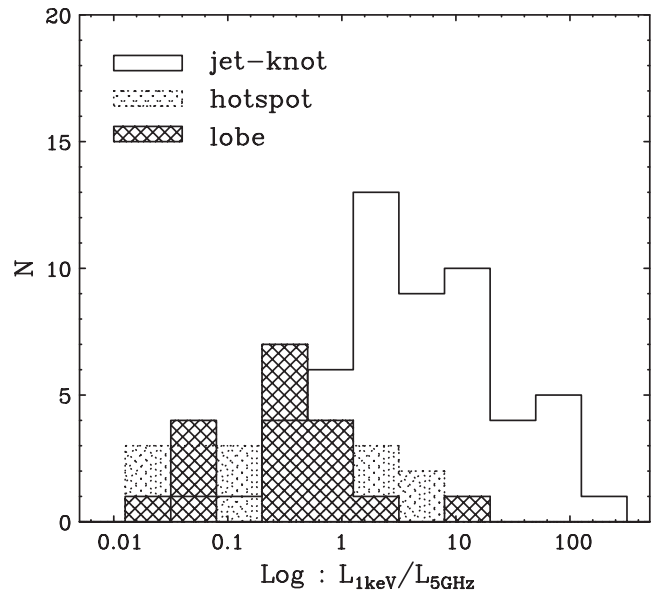


FIG. 2.—Distribution of the ratio between $L_{1\text{keV}}$ and $L_{5\text{GHz}}$.

faint” jet knots. Therefore, the lack of the X-ray–faint (i.e., $L_R \geq L_X$) jet knots at the bottom left corner of Figure 3 would be biased by the sensitivity of the *Chandra* detector. In fact, we can find a few X-ray–faint jet knots at the top right corner, where the luminosity is the highest. However, even if only high-luminosity sources are selected, we can see a clear difference between the jet knots, hot spots, and radio lobes, namely, “X-ray–bright” sources are found only in jet knots. Apparently, this is not due to the sampling effect, since we certainly would have been able to detect X-ray–bright hot spots if they existed.

3. MODEL APPLICATION TO DATA

In this section we present a simple formulation of computing an equipartition magnetic field strength B_{eq} from an observed radio flux f_R measured at a radio frequency ν_R . Next we calculate

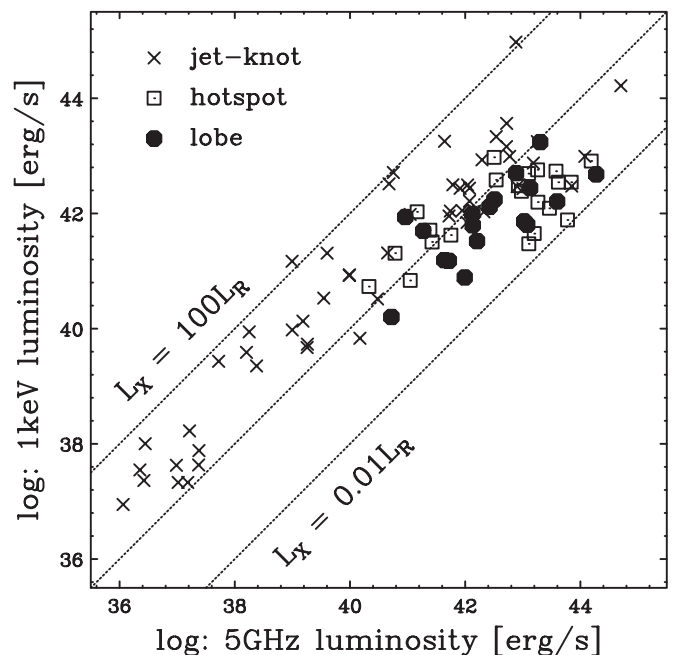


FIG. 3.—Relation between the luminosities $L_{5\text{GHz}}$ and $L_{1\text{keV}}$.

the “expected” SSC and EC luminosities for B_{eq} to compare them with the observed X-ray luminosities. In the analysis, we include possible relativistic bulk velocity of the jet plasma. Taking the obtained results into account, and additionally analyzing the observed broadband spectral properties of the compiled sources (including optical fluxes), we follow the “conservative” classification of the compiled X-ray sources into three groups, namely, (1) synchrotron involving single or broken power-law electron energy distribution (SYN), (2) synchrotron self-Compton (SSC), and (3) external Compton of CMB photons (EC). Finally, we discuss the validity of the applied classification scheme and compare it briefly with the classification introduced in the literature.

3.1. Equipartition Magnetic Field

In order to determine the X-ray emission properties of the large-scale jets, we first estimated the magnetic field strength under the minimum-power hypothesis using the observed radio luminosities measured at 5 GHz. As we review in § 1, it is generally believed that the magnetic field energy density u_B and the particle energy density u_e may be close to equipartition in a number of radio sources. Therefore, our approach is that we first assume an equipartition to calculate “predicted” inverse Compton X-ray luminosities and then compare them to the observed ones. If a large discrepancy occurs, this may suggest that equipartition is strongly violated, that the inverse Compton origin of the observed keV photons is not the case, or that we have to consider another correction factor, such as Doppler beaming factor δ , as we discuss below.

Since the synchrotron luminosity, L_ν , is proportional to $u_e u_B V$, where V is the volume of the emitting regions, we can estimate the equipartition magnetic field B_{eq} for a given luminosity observed at a radio frequency ν . Under the assumption of *no* relativistic beaming ($\delta = 1$), B_{eq} is expressed as

$$B_{\text{eq},\delta=1} = \left[\frac{3\mu_0 G(\alpha)\eta L_\nu}{2V} \right]^{2/7} \propto \left(\frac{\eta L_\nu}{V} \right)^{2/7} \nu^{1/7}, \quad (1)$$

where μ_0 is the permeability of free space, $G(\alpha)$ is a function given in Longair (1994), α is the spectral energy index, L_ν is the synchrotron luminosity measured at a frequency ν , and η is the ratio of energy density carried by protons and electrons to the energy density of the electrons; i.e., $\eta = 1$ for the leptonic (e^-e^+) jet and $\eta = 1836$ for the hadronic (e^-p^+) jet for which the ratio of proton to electron energy densities equals the ratio of their rest masses. In the last approximation in equation (1), we put the minimum synchrotron frequency $\nu_{\text{min}} = \nu$ and $\alpha = 0.75$. The latter choice is justified by a narrow distribution of the radio spectral indexes in the compiled data set (Fig. 1, *top*). The former choice gives the *minimum* value of B_{eq} for the observed L_ν at some given frequency ν . Below we consider $\nu = \nu_R = 5$ GHz, although it is obvious that the minimum radio frequency has to be lower than this (especially in the case of the EC model, which requires the presence of low-energy electrons with energies below GeV scales). However, the difference between the equipartition magnetic field computed for $\nu_{\text{min}} = \nu$ and for $\nu_{\text{min}} \neq \nu$ is rather small, $\propto (\nu_{\text{min}}/\nu)^{1/14}$. In addition, the expected spectral flattenings at the low-energy part of the synchrotron continuum are likely to make this difference even smaller.

In general, an emission volume, V , is quite uncertain for astrophysical sources because of the limited angular resolution of detectors and projection effect. We have assumed that the emitting region has a spherical volume of a certain angular radius θ (in arcseconds) for all the jet structures. This is obviously an

oversimplified assumption; however, it significantly reduces the complexity of the models. Most of the jet knots and hot spots are pointlike sources when observed with *Chandra*. We therefore set an upper limit of $\theta = 0''.3$, unless there are additional radio/optical observations obtained with better angular resolution. Meanwhile, a number of radio lobes show extended structures, but morphology is more complicated than a homogeneous sphere. We therefore calculated the volume by assuming a cylinder or a rotational ellipse and then approximated it as a sphere that has an equal volume.

For a relativistically moving plasma, the equipartition magnetic field measured in the emitting plasma rest frame is related to the equipartition value computed for no beaming by the relation (Stawarz et al. 2003)

$$B_{\text{eq}} = B_{\text{eq},\delta=1} \delta^{-5/7}. \quad (2)$$

The above expression can be more conveniently written as

$$B_{\text{eq}} = 123 \eta^{2/7} (1+z)^{11/7} \left(\frac{d_L}{100 \text{ Mpc}} \right)^{-2/7} \left(\frac{\nu_R}{5 \text{ GHz}} \right)^{1/7} \times \left(\frac{f_R}{100 \text{ mJy}} \right)^{2/7} \left(\frac{\theta}{0''.3} \right)^{-6/7} \delta^{-5/7} \mu\text{G}, \quad (3)$$

where d_L is the luminosity distance to the source and f_R is the observed radio luminosity measured at frequency ν_R . Values of $B_{\text{eq},\delta=1}$ for various jet sources are calculated in Table 2 for $\eta = 1$, which gives again the *minimum* value of $B_{\text{eq},\delta=1}$. We note that this particular choice does not refer exclusively to the leptonic jet model. For example, it may refer to the case of energy equipartition solely between the jet magnetic field and radiating electrons. We note that the discussion on the jet composition is still open, and the situation may be quite complex as, for example, the jet can be composed predominantly from the e^-e^+ pairs but still remain dynamically dominated by the (cold) hadrons (see Sikora & Madejski 2000).

3.2. Synchrotron (SYN) Case

We first consider the case in which the X-ray emissions are due to the synchrotron radiation emitted by the electrons with the Lorentz factor γ_X . We assume that the magnetic field in the jet-moving plasma is close to equipartition B_{eq} and its relativistic beaming factor is δ . Then the observed X-ray frequency is given by

$$\begin{aligned} \nu_X &\simeq 1.2 \times 10^6 \gamma_X^2 B_{\text{eq}} (1+z)^{-1} \delta \\ &\simeq 1.2 \times 10^6 \gamma_X^2 B_{\text{eq},\delta=1} (1+z)^{-1} \delta^{2/7}. \end{aligned} \quad (4)$$

The respective electron Lorentz factor, γ_X , is hence given as

$$\gamma_X \simeq 4.5 \times 10^7 \left(\frac{\nu_X}{\nu_{1 \text{ keV}}} \right)^{1/2} \left(\frac{B_{\text{eq},\delta=1}}{100 \mu\text{G}} \right)^{-1/2} (1+z)^{1/2} \delta^{-1/7}, \quad (5)$$

where $\nu_{1 \text{ keV}}$ is 2.4×10^{17} Hz. Therefore, although δ is quite uncertain, the estimated value of γ_X is not affected significantly, since γ is only weakly dependent on δ ; i.e., $\propto \delta^{-1/7}$.

3.3. Synchrotron Self-Compton (SSC) Emission

The observed radio frequency is approximately

$$\nu_R \simeq 1.2 \times 10^6 B_{\text{eq}} \gamma_R^2 (1+z)^{-1} \delta, \quad (6)$$

where γ_R is the Lorentz factor of the electrons, which emit synchrotron photons at ν_R . In the SSC case, electrons upscatter synchrotron photons to a frequency

$$\begin{aligned}\nu_{\text{IC}} &\simeq \frac{4}{3} \gamma_R^2 \nu_R \\ &= 2.8 \times 10^{17} \left(\frac{\nu_R}{5 \text{ GHz}} \right)^2 \left(\frac{B_{\text{eq}}}{100 \mu\text{G}} \right)^{-1} (1+z) \delta^{-1} \text{ Hz} \\ &= 2.3 \times 10^{17} \eta^{-2/7} (1+z)^{-4/7} \left(\frac{d_L}{100 \text{ Mpc}} \right)^{2/7} \\ &\quad \times \left(\frac{\nu_R}{5 \text{ GHz}} \right)^{13/7} \left(\frac{f_R}{100 \text{ mJy}} \right)^{-2/7} \left(\frac{\theta}{0''.3} \right)^{6/7} \delta^{-2/7} \text{ Hz.} \quad (7)\end{aligned}$$

Note that ν_{IC} depends both on the observed radio frequency and on the magnetic field strength B_{eq} . To calculate the X-ray flux at an observed frequency ν_X , we have to extrapolate the inverse Compton flux calculated for ν_{IC} by assuming the observed X-ray spectral index α_X . In the SSC case, we expect $\alpha_X \simeq \alpha_R$, if the synchrotron continuum can be well-approximated by a single power law with $\alpha \simeq \alpha_R$. The ratio of X-ray (SSC) luminosity to the radio (synchrotron) luminosity is therefore

$$\frac{\nu_{\text{IC}} f_{\text{IC}}}{\nu_R f_R} \simeq \frac{\nu_X f_X}{\nu_R f_R} \left(\frac{\nu_{\text{IC}}}{\nu_X} \right)^{1-\alpha_R} \simeq \frac{u'_{\text{sync}}}{u'_B}, \quad (8)$$

where u'_{sync} and u'_B are the synchrotron photon energy density and the magnetic field density, respectively, both evaluated in the emitting region rest frame denoted by primes. Here u'_{sync} is given by

$$\begin{aligned}u'_{\text{sync}} &= \frac{d_L^2 \nu_R f_R}{R^2 c \delta^4} \\ &= 7.9 \times 10^{-13} (1+z)^4 \left(\frac{\nu_R}{5 \text{ GHz}} \right) \left(\frac{f_R}{100 \text{ mJy}} \right) \\ &\quad \times \left(\frac{\theta}{0''.3} \right)^{-2} \delta^{-4} \text{ ergs cm}^{-3}, \quad (9)\end{aligned}$$

if we assume that the emission regions (jet knots) are *moving* sources (see a discussion in Stawarz et al. 2004). From equations (7)–(9), we predict the SSC flux density measured at ν_X to be roughly

$$\begin{aligned}f_X &= 2.8 \times 10^{-3} \eta^{-1/2} (1+z) \left(\frac{d_L}{100 \text{ Mpc}} \right)^{1/2} \left(\frac{\nu_R}{5 \text{ GHz}} \right)^{5/4} \\ &\quad \times \left(\frac{\nu_X}{\nu_{1 \text{ keV}}} \right)^{-3/4} \left(\frac{f_R}{100 \text{ mJy}} \right)^{3/2} \left(\frac{\theta}{0''.3} \right)^{-1/2} \delta^{-5/2} \text{ nJy.} \quad (10)\end{aligned}$$

Here we have assumed $\alpha_R = 0.75$, taking the result of Figure 1 into account. Note that f_X goes as $\delta^{-5/2}$, meaning that the SSC flux significantly *decreases* as the beaming factor increases. Note also that $f_X \propto \theta^{-1/2}$, i.e., that for a given f_R and $B = B_{\text{eq}}$, clumping of the emission region leads to the *increase* of the SSC X-ray flux.

3.4. External Compton (EC) Emission on Cosmic Microwave Background Photon Field

Similarly to the SSC case, we can estimate the expected EC flux at a certain X-ray frequency ν_X . In the EC model, electrons

upscatter CMB photons to frequencies peaked at ν_{IC} , which, in a Thomson regime, is simply

$$\begin{aligned}\nu_{\text{IC}} &\simeq \frac{4}{3} \gamma_R^2 \nu_{\text{CMB}} (1+z)^{-1} \delta^2 \kappa \\ &= 7.3 \times 10^{18} \eta^{-2/7} \kappa (1+z)^{-4/7} \left(\frac{d_L}{100 \text{ Mpc}} \right)^{2/7} \\ &\quad \times \left(\frac{\nu_R}{5 \text{ GHz}} \right)^{6/7} \left(\frac{f_R}{100 \text{ mJy}} \right)^{-2/7} \left(\frac{\theta}{0''.3} \right)^{6/7} \delta^{12/7} \text{ Hz,} \quad (11)\end{aligned}$$

where $\kappa = (1+\mu)(1+\beta)^{-1}$ and $\nu_{\text{CMB}} = 1.6 \times 10^{11} (1+z) \text{ Hz}$. Here we may set $\kappa \simeq 1$ for simplicity, since the value of κ is always on the order of unity for any choice of Γ_{blk} and δ . The ratio of X-ray (EC) luminosity to the radio (synchrotron) luminosity is approximately given by (Stawarz et al. 2003):

$$\frac{\nu_{\text{IC}} f_{\text{IC}}}{\nu_R f_R} \simeq \frac{\nu_X f_X}{\nu_R f_R} \left(\frac{\nu_{\text{IC}}}{\nu_X} \right)^{1-\alpha_R} \simeq \frac{u_{\text{CMB}}}{u'_B} \kappa^2 (1+z)^4 \delta^2, \quad (12)$$

where $u_{\text{CMB}} = 4.1 \times 10^{-13} \text{ ergs cm}^{-3}$. From equations (11) and (12), the EC flux density measured at ν_X can be expressed as

$$\begin{aligned}f_X &= 5.9 \times 10^{-4} \kappa^{7/4} \eta^{-1/2} (1+z) \left(\frac{d_L}{100 \text{ Mpc}} \right)^{1/2} \left(\frac{\nu_R}{5 \text{ GHz}} \right)^{1/2} \\ &\quad \times \left(\frac{\nu_X}{\nu_{1 \text{ keV}}} \right)^{-3/4} \left(\frac{f_R}{100 \text{ mJy}} \right)^{1/2} \left(\frac{\theta}{0''.3} \right)^{3/2} \delta^3 \text{ nJy} \quad (13)\end{aligned}$$

for $\alpha_R = 0.75$. It is interesting to note that f_X goes as δ^3 , meaning that the EC flux significantly *increases* as the beaming factor increases, which is the exact opposite of the trend in the SSC case. Note also that in the case of the EC emission $f_X \propto \theta^{3/2}$; i.e., for smaller emission region with given f_R and $B = B_{\text{eq}}$, the EC X-ray emission decreases, again opposite to what is expected in the case of the SSC process.

3.5. Source Classification

First we group the sources by the X-ray spectral index α_X and the X-ray flux f_X observed at 1 keV. If the X-ray emission smoothly connects with the radio/optical spectra, we consider the X-rays to be produced via the synchrotron emission as for the radio to optical photons, and that only the highest energy tail of the electron population contributes to the X-ray emission. Good examples are the knots in M87, where the X-ray spectral indexes are $\alpha_X \simeq 1.3$ – 1.6 and the X-ray fluxes are consistent with radio/optical/X-ray synchrotron continua of a broken power law form. As listed in Table 3, we find 25 “synchrotron” jet knots and seven hot spots, but none were found for the radio lobes. Figure 4 plots the distribution of $\gamma_X \delta^{1/7}$, calculated from equation (5) derived in § 3.2. Note that for all the synchrotron sources, electrons must be accelerated very efficiently up to $\gamma_X \simeq 10^7$ – 10^8 for $B = B_{\text{eq}}$ (and to even higher energies if only $B < B_{\text{eq}}$), and that the highest population is occupied by the hot spots.

Meanwhile, remaining sources show flat X-ray spectra that cannot connect smoothly with the radio and optical spectra in terms of a single (or broken) power-law continuum. Let us follow the “conservative” hypothesis that the X-rays in these sources are due to the inverse Compton emission of either synchrotron itself (SSC) or the CMB photons (EC). We therefore compare the ratio between the observed flux density to that expected one from SSC and EC models (cf., §§ 3.3 and 3.4), R_{SSC} and R_{EC} , to determine which process may dominate for the X-ray production. For

TABLE 3
SOURCE CLASSIFICATION OF JETS, HOT SPOTS, AND LOBES

| Class | Jet Knot | Hot Spot | Lobe |
|------------------------------------|----------|----------|------|
| Classification by AGN Type | | | |
| QSO (CD)..... | 19 | 2 | 0 |
| QSO (LD)..... | 7 | 9 | 6 |
| RG (FR I)..... | 22 | 0 | 3 |
| RG (FR II)..... | 1 | 13 | 9 |
| BLZR..... | 7 | 0 | 0 |
| Classification by Emission Process | | | |
| SYN..... | 25 | 7 | 0 |
| SSC..... | 4 | 16 | 1 |
| EC..... | 27 | 1 | 17 |

example, the hot spot of 3C 123 is well explained by SSC, because $R_{\text{SSC}}(1) = 1.5$ and $R_{\text{EC}}(1) = 130$. This means that the observed X-ray luminosity is 1.5 times larger than that expected from the SSC model under the equipartition hypothesis, whereas it is 140 times the expected EC flux if $\delta = 1$. In contrast, a good example of the EC source are the lobes in 3C 15, where $R_{\text{SSC}}(1) = 58$ and $R_{\text{EC}}(1) = 1.1$. The results of classification are given in the last column of Table 2.

The resulting group of jet knots, hot spots, and radio lobes are summarized in Table 3. Note that most of the jet knots are either the synchrotron or the EC sources, whereas the majority of the hot spots are SSC sources. Moreover, almost all the radio lobes emit X-rays via the EC (CMB) process. However, in a number of jet knots classified as SSC and EC, the observed X-ray luminosities cannot be reproduced satisfactorily. For example, modeling of the jet knot in PKS 0637 results in $R_{\text{SSC}}(1) = 600$ and $R_{\text{EC}}(1) = 1600$, meaning that the observed X-ray flux is about 1000 times brighter than those expected from both the EC and SSC models. As we derive in §§ 3.3 and 3.4, and as is well known from the literature, such a discrepancy could be reduced by taking the relativistic beaming effect into account, $\delta \neq 1$, by giving up the equipartition hypothesis, $B < B_{\text{eq}}$, or by

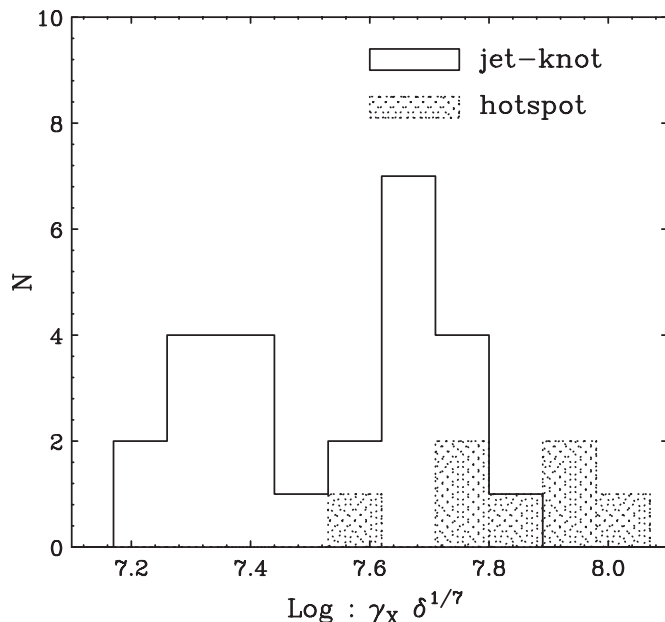


FIG. 4.—Distribution of the electron Lorentz factor, γ_x , for the SYN sources.

postulating a synchrotron origin of the X-ray photons due to an additional flat-spectrum electron population. None of these possibilities can be simply excluded. We comment more about it in § 4.

Let us mention briefly that because of differences in the model-fitting procedure adopted in this paper as compared to the previous studies reported in the literature, some differences may occur in either specific values for the obtained model parameters (e.g., Sambruna et al. [2004] for the case of NGC 6251) or even in classification of some particular sources (e.g., Fabian et al. [2003] for 3C 9). Yet another case is the knot A1 in quasar 3C 273. Marshall et al. (2001) claimed that its X-ray emission is consistent with the extrapolation of the radio-to-optical single power-law synchrotron continuum. However, Jester et al. (2002) have shown that this is not the case, as the observed X-ray flux thereby *exceeds* the one expected from such an extrapolation. Here we classify the 3C 273 knot A1 as the SYN source, in accordance with Marshall et al. (2001), although it should be emphasized that—in face of the detailed optical studies by Jester et al. (2002, 2005)—this particular choice already involves non-standard energy distribution of the radiating electrons.

4. DISCUSSION

In the previous sections, we have followed “conservative” classification of the discussed sources based on their radio and X-ray emission properties. SYN sources are mainly found as jet knots in nearby low-luminosity radio galaxies, in agreement with previous studies (e.g., Hardcastle et al. 2001b; Pesce et al. 2001; Birkinshaw et al. 2002). If the magnetic field strength is not far from the equipartition value in these objects, the electrons must be accelerated very efficiently up to 10–100 TeV, in accordance with the general expectation that radio galaxies may be some of the most efficient particle accelerators in the universe (see a discussion in Kataoka et al. 2003a). If the electrons are actually accelerated to such high energies, the electrons emitting via synchrotron in the X-ray band have relatively short radiative lifetimes. The synchrotron cooling time of the electrons can be expressed as

$$t_{\text{sync}} = 250 \left(\frac{B_{\text{eq}}}{100 \mu\text{G}} \right)^{-2} \left(\frac{\gamma}{10^7} \right)^{-1} \text{ yr.} \quad (14)$$

Since Comptonization of the synchrotron photons, CMB photons, and galactic photon fields also cools electrons (which could be especially significant if the considered jets are relativistic on kiloparsec scales), the above estimate would be an upper limit for the electron cooling timescale. Indeed, Stawarz et al. (2003) estimated the energy density of the starlight emission at 1 kpc from the center of average elliptical galaxy—where the X-ray-bright knots of the low-power jets are typically located—to be $u_{\text{star}} \sim 10^{-9} \text{ ergs cm}^{-3}$. For the 25 FR I jet knots classified as SYN sources in this paper, the median equipartition magnetic field computed for nonrelativistic bulk velocities is $B_{\text{eq}, \delta=1} = 130 \mu\text{G}$ (see Table 2), which gives the comoving energy density of the magnetic field $u'_B = 6.7 \times 10^{-10} \delta^{-10/7} \text{ ergs cm}^{-3}$. Thus, the relative importance of the inverse Compton to synchrotron radiative losses for the electrons within the FR I jets is roughly

$$\frac{u'_{\text{star}}}{u'_B} \sim \Gamma_{\text{blk}}^2 \delta^{10/7}. \quad (15)$$

That is, radiating electrons within nearby FR I jets possessing X-ray (and optical) counterparts (which are believed to be at

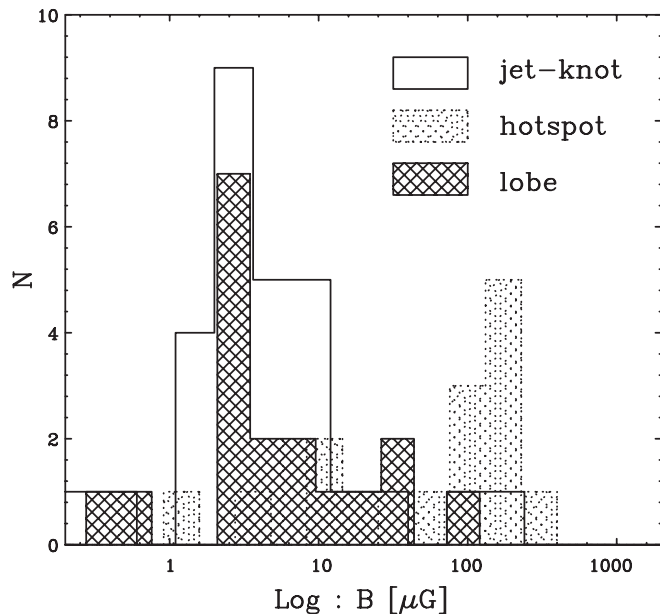


FIG. 5.—Distribution of the evaluated magnetic field, B , for the case of *no* relativistic beaming ($\delta = 1$).

least moderately beamed toward the observer, $\delta > 1$) cool mainly as a result of inverse Compton losses on the starlight photon fields of the host galaxies unless $B \gg B_{\text{eq}}$. Hence, for the highest energy electrons in the FR I jets one can safely put the radiative cooling spatial scale $ct_{\text{cool}} < 100$ pc. In general, this is consistent with the visual sizes of the jet knots but significantly smaller than the typical knots' distances from the nucleus (≥ 1 kpc in the case of FR I sources) and also than the typical interknot separation distances. Therefore, the jet electrons have to be accelerated in situ, most probably because of stochastic processes connected with strong turbulence occurring within those jets as a result of the mass entrainment from the surrounding medium (De Young 1986).

One could ask whether in the case of the SYN jet knots in the nearby FR I galaxies the magnetic field can be much smaller than the equipartition value. This possibility could be verified by means of detecting the inverse Compton radiation of the synchrotron-emitting electrons, which is expected to peak at the high-energy γ -ray band. Interestingly, we can already put some meaningful limits on such a high-energy component in the case of the M87 jet. Nearby radio galaxy M87 was detected at TeV photon energies by the High Energy Gamma Ray Astronomy (HEGRA) Cherenkov Telescope (Aharonian et al. 2003), and it was shown that the kiloparsec-scale jet in this object can produce very high energy γ -ray photons at the required level via Comptonization of the starlight photon field (Stawarz et al. 2003). However, the latest nondetection of M87 by the Whipple Telescope (Le Bohec et al. 2004) suggests variability of the discussed TeV radiation, indicating that the kiloparsec-scale jet in M87 cannot account for the HEGRA signal. The implied upper limits indicate in turn that the magnetic field within the kiloparsec-scale jet of the M87 radio galaxy cannot be smaller than the equipartition value (Stawarz et al. 2005). Thus, one can also expect that in the case of the other FR I jets $B \gtrsim B_{\text{eq}}$.

For the SSC and EC sources, a number of jet knots seem extremely bright in X-rays, as we have seen in Figures 2 and 3. This inevitably causes a large discrepancy between the “expected” and “observed” X-ray fluxes, as we see in Table 2 and § 3.5, and which is again well known from the previous studies. One

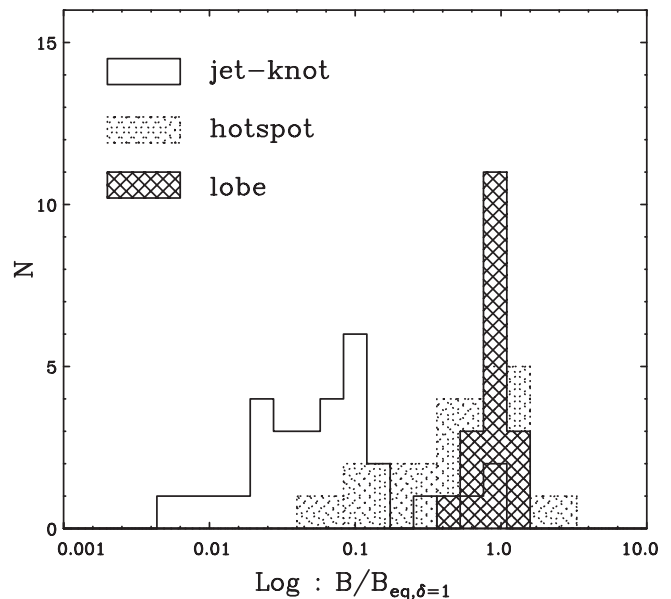


FIG. 6.—Distribution of the ratio between the evaluated magnetic field B (for $\delta = 1$) and the equipartition value $B_{\text{eq},\delta=1}$.

formal possibility is that equipartition hypothesis may not be valid in the considered jet knots. For a given synchrotron luminosity $L_{\text{sync}} \propto u_e u_B$ and for a given emitting region volume V , an expected SSC luminosity is $L_{\text{SSC}} \propto u_e$. We therefore expect the ratio $R_{\text{SSC}}(1) \propto L_{\text{SSC}}^{-1} \propto u_B$. Similarly, for the EC case, $R_{\text{EC}}(1) \propto L_{\text{EC}}^{-1} \propto u_B$. Hence, in both models, the expected X-ray luminosity is increased by decreasing the magnetic field strength.

Figure 5 shows the distribution of the “best-fit” magnetic field B if we allow for the deviation from the equipartition condition and assume nonrelativistic velocities for the emitting regions (which, in the case of the jet knots, is rather only a formal hypothesis). One finds that both the non-SYN jet knots and the radio lobes are distributed around $B \simeq 1\text{--}10 \mu\text{G}$, whereas hot spots have a relatively narrow peak at higher field strength, $B \simeq 50\text{--}300 \mu\text{G}$, plus a “tail” extending down to $\sim 1 \mu\text{G}$. Figure 6 shows the ratio of B to the equipartition value. Interestingly, B in the lobe and most of the hot spots is almost consistent with equipartition ($B/B_{\text{eq},\delta=1} \sim 1$), whereas that of the non-SYN jet knots and of some of the hot spots is much weaker than what is expected ($B/B_{\text{eq},\delta=1} \sim 0.01\text{--}0.1$).

As an alternative idea, we also consider a case in which the difference between the “expected” and “observed” X-ray fluxes is due to the relativistic beaming effect, and the minimum-power condition is fulfilled, as suggested by Tavecchio et al. (2000) and Celotti et al. (2001). Relativistic beaming changes the observed X-ray luminosities significantly as $f_{\chi} \propto \delta^{-5/2}$ for the SSC and $\propto \delta^3$ for the EC (eqs. [10] and [13]). Deviation from equipartition may not be formally required so long as an appropriate beaming factor is assumed. The Doppler factors thus calculated are shown in Table 2 and Figure 7. One can see that the lobes and hot spots exhibit relatively narrow distribution at $\delta \sim 1$, whereas for most of the jet knots large beaming factors of ~ 10 are required, as noted before by many authors. We note that the obtained $\delta \sim 0.1$ for some of the hot spots is rather a formal possibility. Figure 8 shows the distribution of the equipartition magnetic field in the framework of the relativistically moving jet model. Similarly to Figure 5, we find again that the narrowly distributed strength of the magnetic field in the hot spots, $B \sim 100\text{--}500 \mu\text{G}$, is an order of magnitude larger than that of the jet knots and radio lobes.

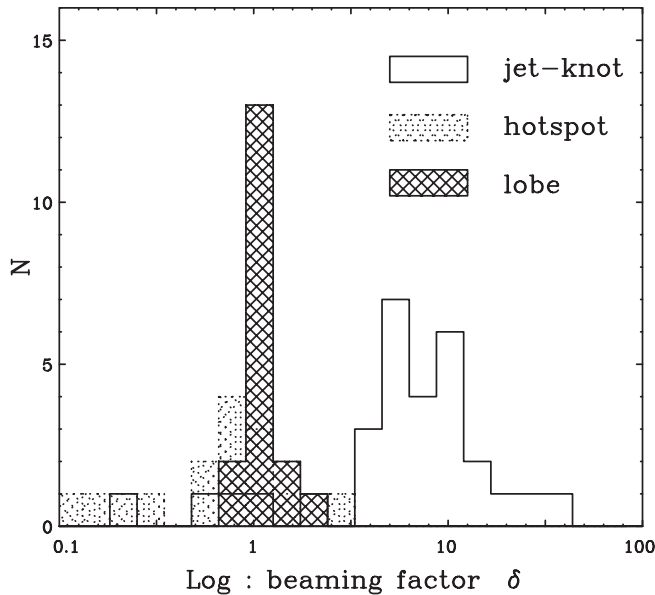


FIG. 7.—Distribution of the required beaming factor δ for $B = B_{\text{eq}}$.

Apparently, the above considerations imply that the inverse Compton X-ray emissions from the lobes and hot spots are relatively close to that expected from the magnetic field–radiating electrons’ energy equipartition, with at most mildly relativistic bulk velocities of the radiating plasma. A number of jet knots in powerful sources require, however, a significant bulk Lorentz factor of $\Gamma_{\text{blk}} \geq \delta/2 \sim 5$ to agree with the inverse Compton origin of the X-ray photons with the minimum-power condition $B = B_{\text{eq}}$. We note that our evaluation gives the *minimum* value of B_{eq} , as we set $\nu_{\text{min}} = \nu$ in equation (1) and $\eta = 1$ in the subsequent analysis. Therefore, any more realistic derivation would result in an even larger deviation from the energy equipartition and thus in an even larger value for the jet Doppler factor δ required to satisfy the minimum-power condition. Let us mention that the alternative two-population synchrotron models do not require violation of the energy equipartition (Stawarz & Ostrowski 2002; Dermer & Atoyan 2004).

Usually, in applying the EC model to the quasar jet knots’ X-ray emission, the idea of subequipartition magnetic field is rejected, since it implies a very high kinetic power of the jets. For this reason, large values for the jet Doppler factors are invoked. However, as discussed by, e.g., Atoyan & Dermer (2004), such an approach does not solve all the problems with the total energy requirements (see also a discussion in Stawarz 2005). Let us mention in this context another important issue. It is well known that the VLA studies of the large-scale jets in quasars and FR II galaxies indicate that bulk Lorentz factors of the radio-emitting plasma in these sources cannot be much greater than $\Gamma_{\text{blk}} \sim 3$ (Wardle & Aaron 1997). The discrepancy between this result and the requirement of the minimum-power EC model for $\Gamma_{\text{blk}} > 10$ is typically ascribed to the jet radial velocity structure, namely that the radio emission originates within the slower moving jet boundary layer, and the inverse Compton X-ray radiation is produced within the fast jet spine (e.g., Ghisellini & Celotti 2001). While it is true that jet radial stratification can indeed significantly influence the jet-counterjet brightness asymmetry ratio, one should be aware that by postulating different sites for the origin of radio and X-ray photons, homogeneous one-zone models for the broadband knots’ emission can no longer be preserved. In particular, in such a case one has to specify, e.g., exactly what fraction of the jet radio emission is produced within the spine and

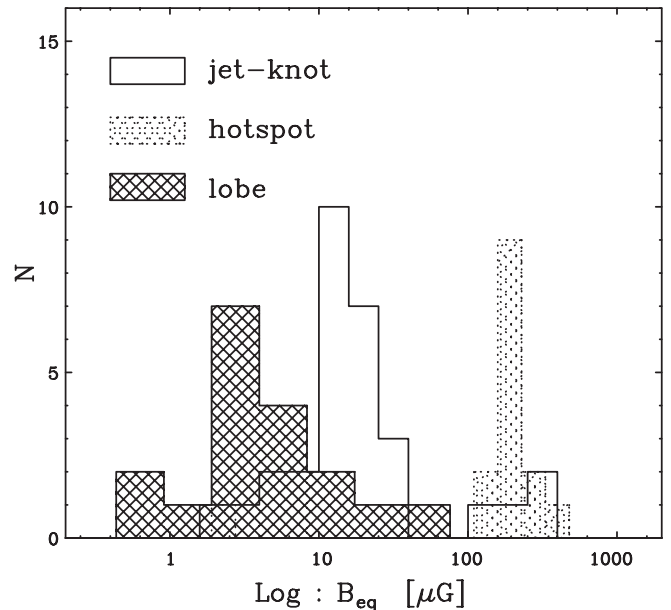


FIG. 8.—Equipartition magnetic field for relativistically moving jet model.

what fraction within the boundary layer, what exactly the jet velocity radial profile is, and what the magnetic field strength is in each jet component. Without such a discussion, one cannot simply use the observed radio flux of the jet to construct the broadband spectral energy distribution of the knot region, i.e., simply estimate the expected inverse Compton flux by means of equipartition magnetic field derived from the radio observations. If one insists on applying the homogeneous one-zone model (as a zero-order approximation), as presented in this paper, self-consistency requires a consideration of $\Gamma_{\text{blk}} \leq 5$. In such a case, a departure from the minimum-power conditions within the non-SYN X-ray jets is *inevitable*.

According to the discussion above, if the X-ray emission of the powerful jets is due to the EC process, these jets are most likely *particle dominated* ($u_e \gg u_B$). The jet magnetic field then must be significantly amplified in the hot spot, where an approximate equipartition is expected to be reached. Then the shocked plasma moves slowly to the radio lobe, where the equipartition field becomes close to the intergalactic value (B of a few μG). Let us comment in this context on the following issue. Pressure of radio-emitting electrons within the lobes of quasars and FR II galaxies computed from the equipartition condition is often found to be below the thermal pressure of the ambient medium (Hardcastle & Worrall 2000), which challenges the standard model for the evolution of powerful radio sources. Such a discrepancy can only be removed by postulating deviations from the equipartition condition or by the presence of nonradiating relativistic protons within the lobes. The presented analysis of the X-ray data confirms, for a large number of sources, the anticipated result that the magnetic field–radiating electrons’ energy equipartition within the lobes is generally fulfilled, and thus that the relativistic protons are very likely to constitute a significant fraction of the lobes’ nonthermal pressure. Interestingly, this would mean that the total energy outputs of powerful jets are systematically *larger* than what is implied solely by the analysis of the lobes’ radio emission (Rawlings & Saunders 1991). This, in turn, would be consistent with deviation from the minimum-power condition within the considered jets themselves. We note that viscous acceleration of cosmic rays taking place at the turbulent boundary layers of relativistic jets,

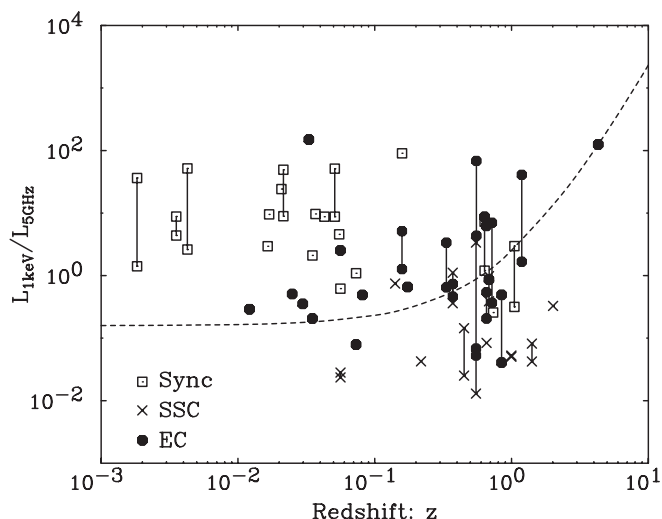


FIG. 9.—Luminosity ratio, $L_{1\text{keV}}/L_{5\text{GHz}}$, as a function of redshift for SYN, SSC, and EC sources.

discussed by, e.g., Ostrowski (2000) and Rieger & Mannheim (2002), could provide an energetically important flat-spectrum population of ultrarelativistic protons within the lobes of powerful radio sources.

We have discussed two different versions of the EC model to account for extremely bright X-ray jet knots: (1) the nonequipartition case and (2) the significant relativistic beaming case. Both of these options are in many ways problematic. Our next concern is to attempt to prove, in general, the postulated inverse Compton origin of the X-ray photons. Note in this context that for the EC sources the radio-to-X-ray flux ratio is proportional to $u_B^{-1}(1+z)^4\delta^2$ (eq. [12]). Therefore, for a large sample of EC sources one should expect to observe $L_R/L_X \propto (1+z)^4$ behavior, if only B and Γ_{blk} do not have large scatter from source to source (cf. Figs. 5 and 7). We therefore expect the high-redshift EC sources to be brighter in X-rays than nearby EC sources (see Schwartz 2002; Cheung 2004).

Figure 9 shows the distribution of the flux ratio ($L_{1\text{keV}}/L_{5\text{GHz}}$) as a function of z . The dotted line shows the $\propto(1+z)^4$ relation that fits the highest z data point (GB 1508+5714, $z = 4.3$) just to help guide the eyes. Although the data sample is still poor, we may say that no clear trend can be seen in this plot. Furthermore, we notice that the discussed ratio is widely distributed even in the same objects. For example, in the cases of the knots in 4C 19.33 ($z = 0.72$), “conservatively” classified as the EC sources, the X-ray-to-radio luminosity ratio changes of about an order of magnitude (Table 2). Such a difference is not easy to explain in the framework of model 1, since we have to assume an order of magnitude increase in the magnetic fields along the jet. In a framework of relativistic beaming (hypothesis 2), one may possibly explain such variation by postulating the decrease of the bulk Lorentz factor along the flow and only moderate changes in magnetic field (Georganopoulos & Kazanas 2004). In this case, however, one has to explain what causes significant deceleration of the jet, which preserves its excellent collimation, with no significant radiative energy losses. We need more data obtained in various energy bands and a more sophisticated analysis to conclude this further. However, we note that recent observations of high-redshift quasars by Bassett et al. (2004) did not reveal any evidence for the enhanced X-ray emission of the distant large-scale jets due to the increased energy density of the CMB. Since such an effect is expected in the framework of the EC model, one may conclude that the X-ray photons from the powerful quasar

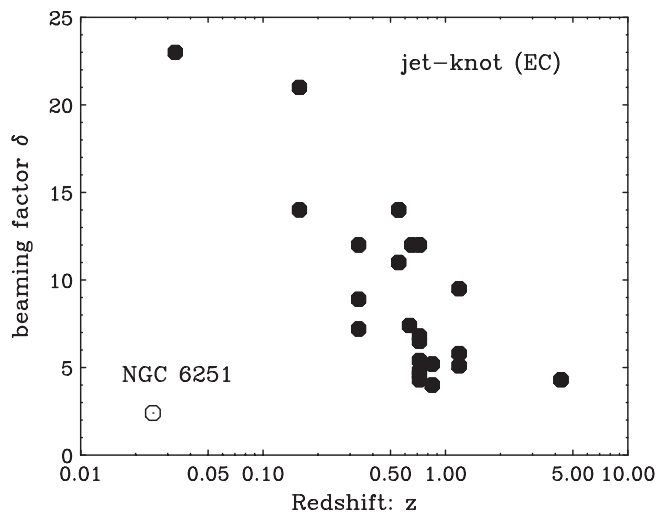


FIG. 10.—Expected beaming factor δ_{EC} for $B = B_{\text{eq}}$ as a function of redshift for EC jet knot sources. The open circle shows FR I radio galaxy NGC 6251, but its X-ray emission seems to be problematic in a framework of the EC model. Full details are given in the text.

jets are not inverse Compton in origin. Recent detailed reanalysis of the *Chandra* data for 3C 120, again “conservatively” classified as an EC source, strongly supports this idea (Harris et al. 2004).

Let us finally discuss yet another issue regarding the EC scenario for the quasar jets’ X-ray emission. Figure 10 shows the Doppler beaming factor δ required in this model to obtain $B = B_{\text{eq}}$ versus the redshifts z of the jet knots classified here as the EC ones. One can clearly see a significant anticorrelation between δ and z , meaning that the high- z sources require much smaller δ for the magnetic field–radiating electrons’ energy equipartition than the sources located closer to the observer.⁵ There are two possible explanations for the noted δ – z anticorrelation. If reflecting a physical property, it would mean that the distant large-scale quasar jets are less relativistic than their nearby analogues but similarly close to the equipartition, or that both low- and high- z quasar jets are only mildly relativistic on large scales but closer to the minimum-power condition when located at large redshifts. Neither of these options appears to be particularly inartificial, especially as the high- z quasar cores seem to be comparable to their low- z counterparts (e.g., Bassett et al. 2004). On the other hand, differences in velocity and energy content of the large-scale jets may not reflect differences in the central engines but more likely differences in the surrounding galactic or intergalactic medium. The second possibility for understanding the δ – z anticorrelation is, however, that it is simply an artifact of the applied but inappropriate EC model. This issue has to be discussed carefully for a larger number of sources.

5. CONCLUSION

We have studied the statistical properties of the large-scale jet knots, hot spots, and lobes in more than 40 radio galaxies recently observed with *Chandra* and *ASCA*. For the jet knots in nearby low-luminosity radio galaxies and for some of the hot spots, X-ray photons are most likely synchrotron in origin, being then produced by ultrarelativistic electrons with energies 10–100 TeV that must be accelerated in situ. For the other

⁵ Nearby FR I radio galaxy NGC 6251 (Fig. 10, open circle) constitutes the only exception from this trend. However, this peculiar source does not belong to the quasar class, and, in general, its X-ray emission is particularly problematic (especially in a framework of the EC model).

objects, X-ray photons are inverse Compton in origin or, alternatively, are due to synchrotron emission of very high energy electrons with a nonstandard energy distribution. In this paper we examine in more detail the former possibility. We first calculated the “expected” SSC or EC fluxes by assuming equipartition magnetic field and nonrelativistic velocity of the emitting plasma and then compared them to the observed fluxes. We confirmed that the observed X-ray fluxes from the hot spots and radio lobes are approximately consistent with the expected ones, whereas a number of the jet knots in powerful sources are too bright at X-rays. We examined two possibilities to account for this discrepancy in a framework of the inverse Compton model. The first idea is that the equipartition hypothesis may not be valid for the considered sources. In this case, the X-ray–bright jets are particle dominated and therefore far from the minimum-power condition. The jet magnetic field must then be significantly amplified in the hot spots, where an approximate energy equipar-

tion with the radiating particles is expected to be reached. An alternative idea is that the jets are highly relativistic ($\Gamma_{\text{blk}} \geq 5$) even on kiloparsec and megaparsec scales but significantly decelerate in the hot spots. This, however, in addition to other problems, challenges the homogeneous one-zone emission region model adopted in this paper, as discussed in the text. Unfortunately, the comparison of the observed radio-to-X-ray flux ratios for various z sources *from the compiled data set* does not provide definite constraints on the X-ray emission process dominating within the quasar and FR II jets.

We would like to thank F. Takahara and M. Ostrowski for fruitful discussion and constructive comments. J. K. acknowledges a support by JSPS.KAKENHI (14340061). Ł. S. was supported by the grants 1-P03D-011-26 and PBZ-KBN-054/P03/2001 and partly by the *Chandra* grants G02-3148A and G0-09280.01-A.

REFERENCES

- Aharonian, F. A. 2002, *MNRAS*, 332, 215
 Aharonian, F. A., et al. 2003, *A&A*, 403, L1
 Akujor, C. E., Spencer, R. E., Zhang, F. J., Davis, R. J., Browne, I. W. A., & Fanti, C. 1991, *MNRAS*, 250, 215
 Aldcroft, T. L., Siemiginowska, A., Elvis, M., Mathur, S., Nicastro, F., & Murray, S. S. 2003, *ApJ*, 597, 751
 Aloy, M. A., Ibáñez, J. M., Martí, J. M., Gómez, J.-L., & Müller, E. 1999, *ApJ*, 523, L125
 Atoyan, A. M., & Dermer, C. D. 2004, *ApJ*, 613, 151
 Bałucińska-Church, M., Ostrowski, M., Stawarz, Ł., & Church, M. J. 2005, *MNRAS*, 357, L6
 Bassett, L. C., Brandt, W. N., Schneider, D. P., Vignali, C., Chartas, G., & Garmire, G. P. 2004, *AJ*, 128, 523
 Birkinshaw, M., Worrall, D. M., & Hardcastle, M. J. 2002, *MNRAS*, 335, 142
 Blundell, K. M., & Rawlings, S. 2000, *AJ*, 119, 1111
 Bridle, A. H., Hough, D. H., Lonsdale, C. J., Burns, J. O., & Laing, R. A. 1994, *AJ*, 108, 766
 Brunetti, G., Bondi, M., Comastri, A., Pedani, M., Varano, S., Setti, G., & Hardcastle, M. J. 2001a, *ApJ*, 561, L157
 Brunetti, G., Bondi, M., Comastri, A., & Setti, G. 2002, *A&A*, 381, 795
 Brunetti, G., Cappi, M., Setti, G., Feretti, L., & Harris, D. E. 2001b, *A&A*, 372, 755
 Brunetti, G., Setti, G., & Comastri, A. 1997, *A&A*, 325, 898
 Celotti, A., Ghisellini, G., & Chiaberge, M. 2001, *MNRAS*, 321, L1
 Chartas, G., Gupta, V., Garmire, G., Jones, C., Falco, E. E., Shapiro, I. I., & Tavecchio, F. 2002, *ApJ*, 565, 96
 Chartas, G., et al. 2000, *ApJ*, 542, 655
 Cheung, C. C. 2004, *ApJ*, 600, L23
 Comastri, A., Brunetti, G., Dallacasa, D., Bondi, M., Pedani, M., & Setti, G. 2003, *MNRAS*, 340, L52
 Dermer, C. D., & Atoyan, A. M. 2002, *ApJ*, 568, L81
 ———. 2004, *ApJ*, 611, L9
 De Young, D. S. 1986, *ApJ*, 307, 62
 ———. 2002a, *NewA Rev.*, 46, 393
 ———. 2002b, *The Physics of Extragalactic Radio Sources* (Chicago: Univ. Chicago Press)
 Donahue, M., Daly, R. A., & Horner, D. J. 2003, *ApJ*, 584, 643
 Fabian, A. C., Celotti, A., & Johnstone, R. M. 2003, *MNRAS*, 338, L7
 Georganopoulos, M., & Kazanas, D. 2004, *ApJ*, 604, L81
 Ghisellini, G., & Celotti, A. 2001, *MNRAS*, 327, 739
 Hardcastle, M. J., Alexander, P., Pooley, G. G., & Riley, J. M. 1997, *MNRAS*, 288, 859
 Hardcastle, M. J., Birkinshaw, M., Cameron, R. A., Harris, D. E., Looney, L. W., & Worrall, D. M. 2002b, *ApJ*, 581, 948
 Hardcastle, M. J., Birkinshaw, M., & Worrall, D. M. 2001a, *MNRAS*, 323, L17
 ———. 2001b, *MNRAS*, 326, 1499
 Hardcastle, M. J., Harris, D. E., Worrall, D. M., & Birkinshaw, M. 2004, *ApJ*, 612, 729
 Hardcastle, M. J., & Worrall, D. M. 2000, *MNRAS*, 319, 562
 Hardcastle, M. J., Worrall, D. M., Birkinshaw, M., Laing, R. A., & Bridle, A. H. 2002a, *MNRAS*, 334, 182
 Harris, D. E., Finoguenov, A., Bridle, A. H., Hardcastle, M. J., & Laing, R. A. 2002a, *ApJ*, 580, 110
 Harris, D. E., Hjorth, J., Sadun, A. C., Silverman, J. D., & Vestergaard, M. 1999, *ApJ*, 518, 213
 Harris, D. E., & Krawczynski, H. 2002, *ApJ*, 565, 244
 Harris, D. E., Krawczynski, H., & Taylor, G. B. 2002b, *ApJ*, 578, 60
 Harris, D. E., Leighly, K., & Leahy, J. P. 1998, *ApJ*, 499, L149
 Harris, D. E., Mossman, A. E., & Walker, R. C. 2004, *ApJ*, 615, 161
 Harris, D. E., et al. 2000, *ApJ*, 530, L81
 Harvanek, M., Stocke, J. T., Morse, J. A., & Rhee, G. 1997, *AJ*, 114, 2240
 Isobe, N. 2002, Ph.D. thesis, Univ. Tokyo
 Isobe, N., Tashiro, M., Makishima, K., Iyomoto, N., Suzuki, M., Murakami, M., Mori, M., & Abe, K. 2002, *ApJ*, 580, L111
 Jester, S. 2003, *NewA Rev.*, 47, 427
 Jester, S., Röser, H.-J., Meisenheimer, K., & Perley, R. 2002, *A&A*, 385, L27
 ———. 2005, *A&A*, 2005, A&A, 431, 477
 Kaiser, C. R. 2000, *A&A*, 362, 447
 Kataoka, J., Edwards, P., Georganopoulos, M., Takahara, F., & Wagner, S. 2003a, *A&A*, 399, 91
 Kataoka, J., Leahy, J. P., Edwards, P. G., Kino, M., Takahara, F., Serino, Y., Kawai, N., & Martel, A. R. 2003b, *A&A*, 410, 833
 Kirk, J. G., & Duffy, P. 1999, *J. Phys. G*, 25, R163
 Komissarov, S. S. 1999, *MNRAS*, 308, 1069
 Kraft, R. P., Forman, W. R., Jones, C., Murray, S. S., Hardcastle, M. J., & Worrall, D. M. 2002, *ApJ*, 569, 54
 Laing, R. A., & Bridle, A. H. 2002, *MNRAS*, 336, 328
 Leahy, J. P., Black, A. R. S., Dennett-Thorpe, J., Hardcastle, M. J., Komissarov, S., Perley, R. A., Riley, J. M., & Scheuer, P. A. G. 1997, *MNRAS*, 291, 20
 Le Bohec, S., et al. 2004, *ApJ*, 610, 156
 Longair, M. S. 1994, *High Energy Astrophysics* (Cambridge: Cambridge Univ. Press)
 Manolakou, K., & Kirk, J. G. 2002, *A&A*, 391, 127
 Marshall, H. L., Miller, B. P., Davis, D. S., Perlman, E. S., Wise, M., Canizares, C. R., & Harris, D. E. 2002, *ApJ*, 564, 683
 Marshall, H. L., et al. 2001, *ApJ*, 549, L167
 Martí, J. M., Müller, E., Font, J. A., Ibáñez, J. M., & Marquina, A. 1997, *ApJ*, 479, 151
 Meisenheimer, K., Yates, M. G., & Röser, H.-J. 1997, *A&A*, 325, 57
 Mizuta, A., Yamada, S., & Takabe, H. 2004, *ApJ*, 606, 804
 Ostrowski, M. 2000, *MNRAS*, 312, 579
 ———. 2002, *J. Phys. Stud.*, 6, 393
 Perlman, E. S., Biretta, J. A., Sparks, W. B., Macchetto, F. D., & Leahy, J. P. 2001, *ApJ*, 551, 206
 Pesce, J. E., Sambruna, R. M., Tavecchio, F., Maraschi, L., Cheung, C. C., Urry, C. M., & Scarpa, R. 2001, *ApJ*, 556, L79
 Rawlings, S., & Saunders, R. 1991, *Nature*, 349, 138
 Rieger, F. M., & Mannheim, K. 2002, *A&A*, 396, 833
 Sambruna, R. M., Gliozzi, M., Donato, D., Tavecchio, F., Cheung, C. C., & Mushotzky, R. F. 2004, *A&A*, 414, 885
 Sambruna, R. M., Maraschi, L., Tavecchio, F., Urry, C. M., Cheung, C. C., Chartas, G., Scarpa, R., & Gambill, J. K. 2002, *ApJ*, 571, 206
 Sambruna, R. M., Urry, C. M., Tavecchio, F., Maraschi, L., Scarpa, R., Chartas, G., & Muxlow, T. 2001, *ApJ*, 549, L161
 Scarpa, R., & Urry, C. M. 2002, *NewA Rev.*, 46, 405
 Schwartz, D. A. 2002, *ApJ*, 569, L23
 Schwartz, D. A., et al. 2000, *ApJ*, 540, L69
 Siemiginowska, A., Bechtold, J., Aldcroft, T. L., Elvis, M., Harris, D. E., & Dobrzycki, A. 2002, *ApJ*, 570, 543

- Siemiginowska, A., Smith, R. K., Aldcroft, T. L., Schwartz, D. A., Paerels, F., & Petric, A. O. 2003a, *ApJ*, 598, L15
- Siemiginowska, A., et al. 2003b, *ApJ*, 595, 643
- Sikora, M., & Madejski, G. 2000, *ApJ*, 534, 109
- Sparks, W. B., Golombek, D., Baum, S. A., Biretta, J., de Koff, S., Macchetto, F., McCarthy, P., & Miley, G. K. 1995, *ApJ*, 450, L55
- Stawarz, L. 2005, *Chinese J. Astron. Astrophys.*, in press (astro-ph/0310795)
- Stawarz, L., & Ostrowski, M. 2002, *ApJ*, 578, 763
- Stawarz, L., Siemiginowska, A., Ostrowski, M., & Sikora, M. 2005, *ApJ*, submitted (astro-ph/0501597)
- Stawarz, L., Sikora, M., & Ostrowski, M. 2003, *ApJ*, 597, 186
- Stawarz, L., Sikora, M., Ostrowski, M., & Begelman, M. C. 2004, *ApJ*, 608, 95
- Tashiro, M., Makishima, K., Iyomoto, N., Isobe, N., & Kaneda, H. 2001, *ApJ*, 546, L19
- Tashiro, M., et al. 1998, *ApJ*, 499, 713
- Tavecchio, F., Maraschi, L., Sambruna, R. M., & Urry, C. M. 2000, *ApJ*, 544, L23
- Wardle, J. F. C., & Aaron, S. E. 1997, *MNRAS*, 286, 425
- Wilson, A. S., & Yang, Y. 2002, *ApJ*, 568, 133
- Wilson, A. S., Young, A. J., & Shopbell, P. L. 2000, *ApJ*, 544, L27
- . 2001, *ApJ*, 547, 740
- Worrall, D. M., Birkinshaw, M., & Hardcastle, M. J. 2001, *MNRAS*, 326, L7
- . 2003, *MNRAS*, 343, L73
- Yuan, W., Fabian, A. C., Celotti, A., & Jonker, P. G. 2003, *MNRAS*, 346, L7